Cell Reports

Article

HNRNPU facilitates antibody class-switch recombination through C-NHEJ promotion and R-loop suppression

Graphical abstract

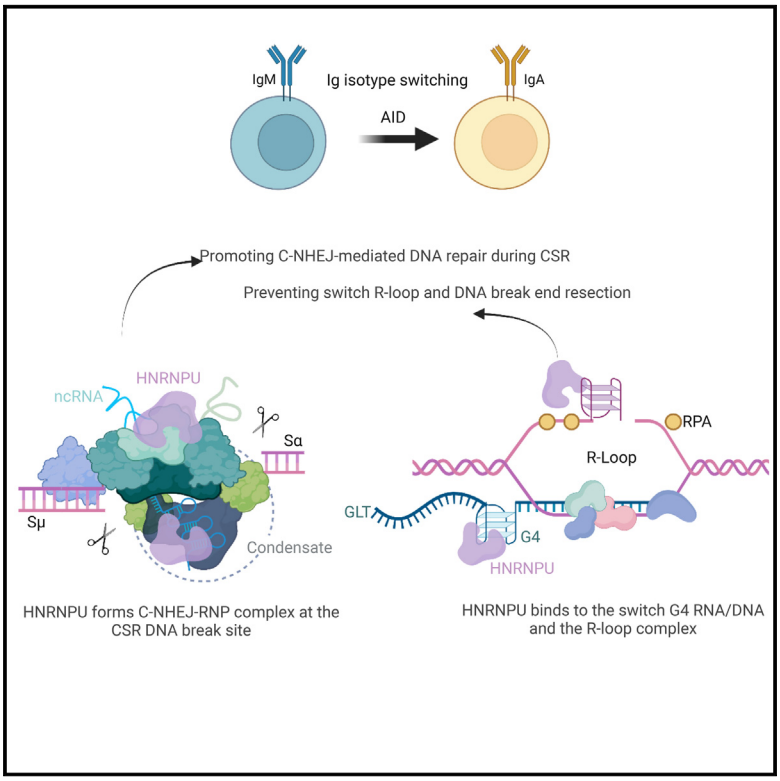

Authors

Ahmed M. Refaat, Mikiyo Nakata, Afzal Husain, Hidetaka Kosako, Tasuku Honjo, Nasim A. Begum

Correspondence

honjo@mfour.med.kyoto-u.ac.jp

In brief

DNA break resolution by C-NHEJ repair plays a crucial role in Ig isotype switching and genomic integrity. Antigen-stimulated B lymphocytes express AID, which induces DNA breaks on actively transcribed Ig gene loci, forming R-loops. Refaat et al. show that HNRNPU loss causes R-loop and C-NHEJ dysregulation, thereby halting AID-induced recombination.

Highlights

- HNRNPU forms a ribonucleoprotein complex with C-NHEJ repair factors
- The RGG/IDR domain of HNRNPU binds to switch RNA/DNA G-quadruplexes
- Loss of HNRNPU increases DNA:RNA hybrids and ssDNA accumulation at the IgH locus
- Liquid-liquid phase separation interference perturbs HNRNPU/C-NHEJ complex occupancy

Refaat et al., 2023, Cell Reports *42*, 112284
March 28, 2023
https://doi.org/10.1016/j.celrep.2023.112284

CellPress

Cell Reports

CellPress
OPEN ACCESS

Article

HNRNPU facilitates antibody class-switch recombination through C-NHEJ promotion and R-loop suppression

Ahmed M. Refaat,[1,2] Mikiyo Nakata,[1] Afzal Husain,[3] Hidetaka Kosako,[4] Tasuku Honjo,[1,5,*] and Nasim A. Begum[1]
[1]Department of Immunology and Genomic Medicine, Center for Cancer Immunotherapy and Immunobiology, Kyoto University Graduate School of Medicine, Kyoto 606-8501, Japan
[2]Zoology Department, Faculty of Science, Minia University, El-Minia 61519, Egypt
[3]Department of Biochemistry, Faculty of Life Sciences, Aligarh Muslim University, Aligarh, Uttar Pradesh 202002, India
[4]Division of Cell Signaling, Institute of Advanced Medical Sciences, University of Tokushima, Tokushima 770-8503, Japan
[5]Lead contact
*Correspondence: honjo@mfour.med.kyoto-u.ac.jp
https://doi.org/10.1016/j.celrep.2023.112284

SUMMARY

B cells generate functionally different classes of antibodies through class-switch recombination (CSR), which requires classical non-homologous end joining (C-NHEJ) to join the DNA breaks at the donor and acceptor switch (S) regions. We show that the RNA-binding protein HNRNPU promotes C-NHEJ-mediated S-S joining through the 53BP1-shieldin DNA-repair complex. Notably, HNRNPU binds to the S region RNA/DNA G-quadruplexes, contributing to regulating R-loop and single-stranded DNA (ssDNA) accumulation. HNRNPU is an intrinsically disordered protein that interacts with both C-NHEJ and R-loop complexes in an RNA-dependent manner. Strikingly, recruitment of HNRNPU and the C-NHEJ factors is highly sensitive to liquid-liquid phase separation inhibitors, suggestive of DNA-repair condensate formation. We propose that HNRNPU facilitates CSR by forming and stabilizing the C-NHEJ ribonucleoprotein complex and preventing excessive R-loop accumulation, which otherwise would cause persistent DNA breaks and aberrant DNA repair, leading to genomic instability.

INTRODUCTION

Expression of activation-induced cytidine deaminase (AID) in antigen-stimulated B lymphocytes diversifies the Ig heavy chain (*IgH*) gene locus through somatic hypermutation (SHM) and class-switch recombination (CSR).[1,2] Whereas error-prone repair of AID-induced DNA breaks in the variable (V) region results in SHM, non-homologous end joining (NHEJ)-mediated DNA repair of AID-induced DNA double-strand breaks (DSBs) in the donor and acceptor switch (S) regions results in CSR.[3,4] During S-S recombination, the paired S region DSBs come into proximity, presumably through a process known as synapsis, followed by DSB end processing and ligation of the DNA break ends, which takes place mainly through classical NHEJ (C-NHEJ) that requires minimal or no sequence homology between two ligating DNA ends.[5,6]

B cells deficient in one of the C-NHEJ components, such as KU80, XRCC4, Ligase IV, 53BP1, or shieldin complex proteins, show compromised CSR and loss of the C-NHEJ signature at CSR junctions.[7–11] During CSR, 53BP1-bound chromatin promotes ataxia telangiectasia mutated (ATM)-dependent recruitment of RIF1, which blocks DNA end resection by recruiting the shieldin complex (SHLD1, SHLD2, SHLD3, and REV7) at the DSB site.[12–14] Because C-NHEJ plays a pivotal role in the resolution of AID-induced S region DSBs, any impairment or alteration of the pathway influences CSR and associated genomic instability.[5,15] Although the defect of C-NHEJ is compensated by an alternative end-joining (A-EJ) DNA-repair pathway, it is less efficient and leads to decreased CSR.[16,17] Therefore, *cis*- and *trans*-acting factors that influence the choice of DNA-repair pathway during CSR are of great importance.

Recent advances in the field suggest that DNA damage itself can generate transient R-loop/DNA:RNA hybrids at DSB sites through the activation of local transcription, promoting DNA repair by providing a recruitment platform for DNA-repair factors.[18–20] The RNAs at the DNA break can influence DNA repair by inviting RNA-binding proteins (RBPs) that are responsive to DNA damage or acting as a template for DNA repair.[21,22] It is well documented that *IgH* S region sequences are highly repetitive and G-rich on the non-template strand and thus frequently form R-loops during S germline transcription.[23,24] The R-loop structure consists of DNA:RNA hybrids on the transcribed strand and single-stranded DNA (ssDNA) on the non-template strand. The displaced ssDNA can form non-B structures, including G-quadruplexes (G4s) and stem-loops that are substrates of S region DNA breaks.[3,4,25] Persistent R-loops can be potentially deleterious because of increased incidents of AID- or other pathway-induced DNA breaks, leading to genomic instability.[26,27] Unscheduled and/or unresolved R-loops can also impair DNA-repair efficiency by obstructing the binding of

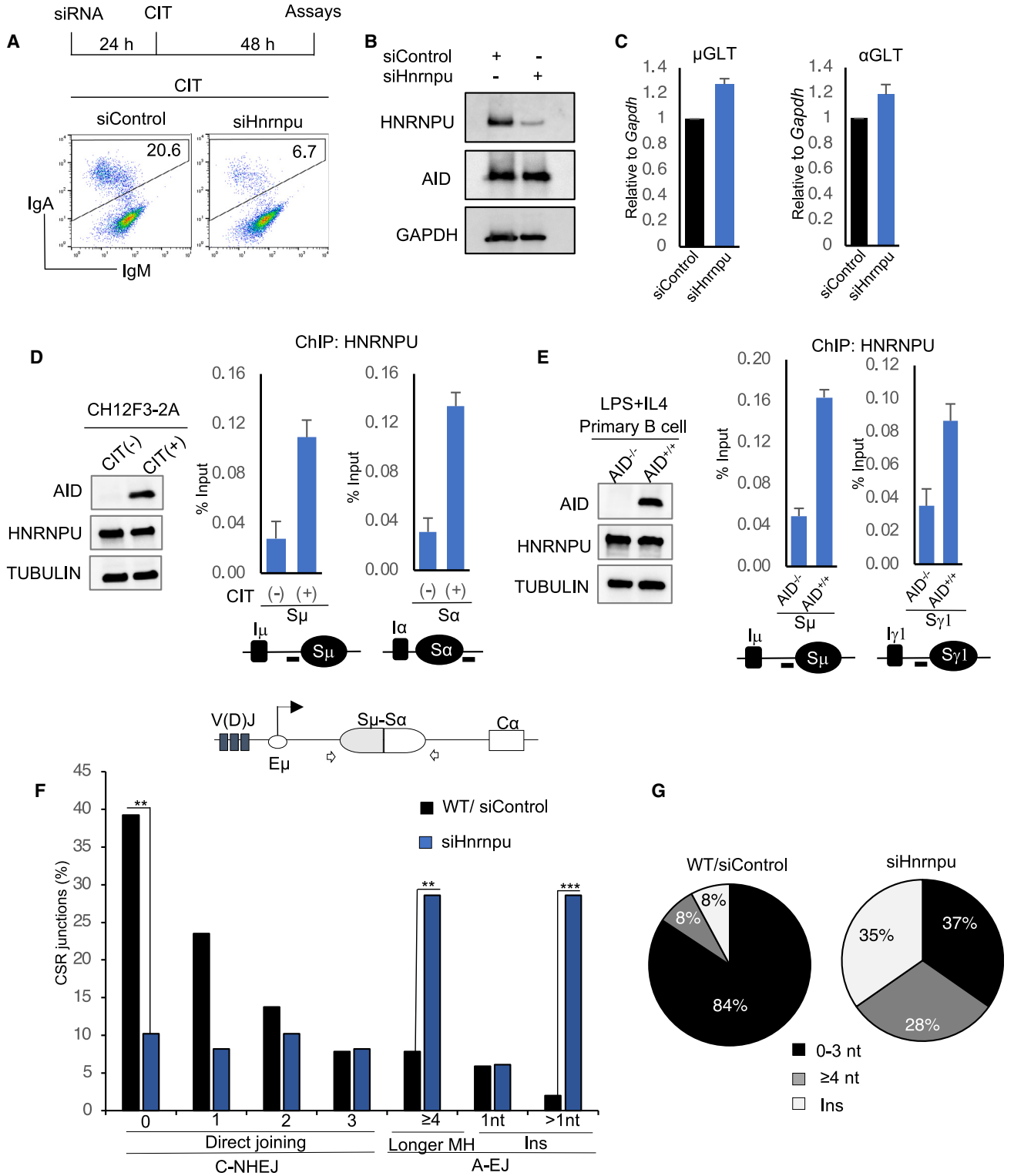

Figure 1. HNRNPU promotes CSR through C-NHEJ

(A) Top: scheme of the IgA-switching assay in CH12F3-2A cells. Bottom: representative FACS profiles of IgA switching in siControl- and siHnrnpu-transfected CH12F3-2A cells stimulated with CIT for 24 h.

(B) Western blot of whole-cell extracts from stimulated CH12F3-2A cells transfected with siControl or siHnrnpu.

(C) Quantitative RT-PCR of μGLT and αGLT from the indicated samples. The values are the mean ± SD (n = 3).

(legend continued on next page)

DNA-repair factors to DSB sites and interfering with the DSB end processing necessary for C-NHEJ. R-loops are particularly beneficial in homologous recombination (HR) because cleavage of the R-loops can generate long 3′ ssDNAs, which are perfect substrates for template DNA invasion during HR.[28,29] It has been reported that RNA processing and modification defects associated with the S region could lead to DNA:RNA hybrid accumulation and suppression, respectively.[30,31] In both cases, AID targeting was affected, and CSR junctions showed elevated microhomology (MH).

In the context of the *IgH* locus, bidirectional transcription-induced S region R-loops are mainly implicated in AID-induced S region DNA breaks, although a role of R-loops in S-S synapsis has also been suggested.[32,33] Recently, it has been shown that G4 structure resolution in S-germline transcripts (GLTs) by the RNA helicase DDX1 promotes R-loops, which correlates with AID recruitment and CSR efficiency.[34] Another study showed that an m6A modification to Sμ-GLT promotes G4 resolution and R-loop formation, again correlating with AID recruitment and CSR efficiency.[31] All studies point to a positive relationship between the S region R-loop and DSB formation. Here, we show that HNRNPU (Q00839), a G4 and DNA/RNA structure-binding protein,[35,36] plays a critical role during CSR at the cross-roads of R-loop and C-NHEJ regulation. The analysis of S-S recombination in HNRNPU-depleted cells showed the hallmark of C-NHEJ defects, accompanied by elevated R-loops and ssDNA in the recombining S regions.

RESULTS

CSR requires HNRNPU to promote C-NHEJ

We initially identified HNRNPU as a CSR cofactor during a screen of HNRNP family genes involved in CSR.[37,38] To investigate the function of HNRNPU in CSR, we knocked down (KD) *Hnrnpu* by introducing a small interfering RNA (siRNA) into the murine B cell line, CH12F3-2A, which undergoes IgM-to-IgA class switching in response to CIT (αCD40/IL4 [interleukin-4]/TGF-β [transforming growth factor beta]) stimulation.[39] As evident in the fluorescence-activated cell sorting (FACS) profiles, HNRNPU-depleted cells showed a marked reduction in IgA switching after 24 h of CIT stimulation, and CSR was impaired even at 72 h (Figures 1A, S1A, and S1B). *Hnrnpu*^{KD} had no apparent effect on AID expression or switch germline transcription (μGLT and αGLT), the essential prerequisites for CSR initiation at the *IgH* locus (Figures 1B and 1C). Similarly, HNRNPU depletion in primary B cells also hindered IgG1 switching without affecting AID and GLT expression (Figures S1D–S1F). A marked elevation of HNRNPU at the S regions was also observed in both CH12F3-2A and wild-type (WT) primary B cells in response to CSR activation or AID (Figures 1D and 1E). However, *Hnrnpu*^{KD} did not perturb AID-induced S region DNA breaks (Figure S3H), suggesting its role is in the DNA-repair phase of CSR.[38]

The recombination phase of CSR requires either the C-NHEJ pathway or the A-EJ pathway to join the cleaved acceptor and donor S regions.[40,41] To investigate the impact of *Hnrnpu*^{KD} on the choice of repair pathway, we PCR amplified and sequenced the Sμ-Sα recombination junctions in WT and HNRNPU-depleted cells stimulated with CIT for 48 h. Sequence analysis of the CSR junctions revealed a striking reduction in direct/blunt end joining and an increase in longer MH at the CSR junctions in HNRNPU-depleted cells (Figure 1F). In WT, most sequenced junctions (84%) showed no MH (0 nt) and short MH (≤3 nt), typical of C-NHEJ and denoted as "direct joining" (Figures 1F and 1G). However, in HNRNPU-depleted cells, 37% and 28% of the sequenced recombination junctions showed 0–3 nt and ≥4 nt MH, respectively (Figures 1F and 1G). HNRNPU-depleted cells also displayed a significantly higher frequency of junctions with insertions (Ins; WT vs. *Hnrnpu*^{KD}: 8% vs. 35%) (Figure 1G), with a marked elevation of >1-nt Ins (Figure 1F). Collectively, these findings suggest that HNRNPU functions primarily to promote C-NHEJ during CSR.

CSR junctions are similar between HNRNPU and shieldin deficiencies

To investigate the nature of the C-NHEJ defect in *Hnrnpu*^{KD} cells, we compared HNRNPU deficiency with 53BP1 and shieldin-component deficiencies within a unified system (CH12F3-2A cells) under identical CSR activation conditions (CIT-induced IgM-to-IgA switching). We used a previously reported three-gene knockout (KO) CH12F3-2A line: *53bp1*^{KO}, *Shld1*^{KO}, and *Shld3*^{KO}.[42] In agreement with previous reports, *53bp1*^{KO} cells showed significant IgA CSR impairment (Figures 2A and S1G).[42,43] There was also a modest decrease in direct joining (0–3 nt; 84% vs. 62%) in the Sμ-Sα junctions with an increase in MH usage (≥4 nt; 8% vs. 13%) compared with WT/siControl-treated cells (Figures 2C and 2F). Interestingly, depletion of *Hnrnpu* in *53bp1*^{KO} cells further reduced direct joining (0–3 nt; 62%–38%) at the CSR junctions (Figure 2F). When we compared the number of junctions with longer MHs, we observed a significant shift toward MH-mediated repair in *53bp1*^{KO} cells on *Hnrnpu* depletion (≥4 nt; 13%–30%) and slight elevation of total Ins (25%–32%) (Figure 2F).

Consistent with previous studies, cells deficient in shieldin subunits showed strongly impaired IgA CSR compared with WT/siControl-treated cells (Figures 2B and S1I). The co-depletion of HNRNPU and shieldin subunits did not reduce CSR further (Figures 2B and S1I–S1K). In *Shld1*^{KO} and *Shld2*^{KD} cells, 48% and 47% of the sequenced recombination junctions showed direct joining (0–3 nt), respectively, which is closer to what we observed in *Hnrnpu*^{KD} cells (37%). Notably, there was

(D and E) HNRNPU occupancy at the recombing S regions during IgA and IgG1 switching in CH12F3-2A (D) and primary B cells (E), respectively. Western blots show the expression of HNRNPU and AID in the whole-cell extracts. The black bars below the plots show the position selected for the chromatin immunoprecipitation (IP; ChIP) assay. The values are means ± SD (n = 3).

(F) Top: schematic representation of the Sμ-Sα junction analysis. Bottom: bar graphs quantifying the distribution of junction features of Sμ-Sα recombination in genomic DNA isolated from CIT-stimulated CH12F3-2A cells after transfection with siControl or siHnrnpu. Statistical significance, according to Fisher's exact test, is shown. The values are presented as mean ± SD (n = 3).

(G) Pie charts showing the distribution of Sμ-Sα junction features derived from control and HNRNPU knockdown (KD) cells.

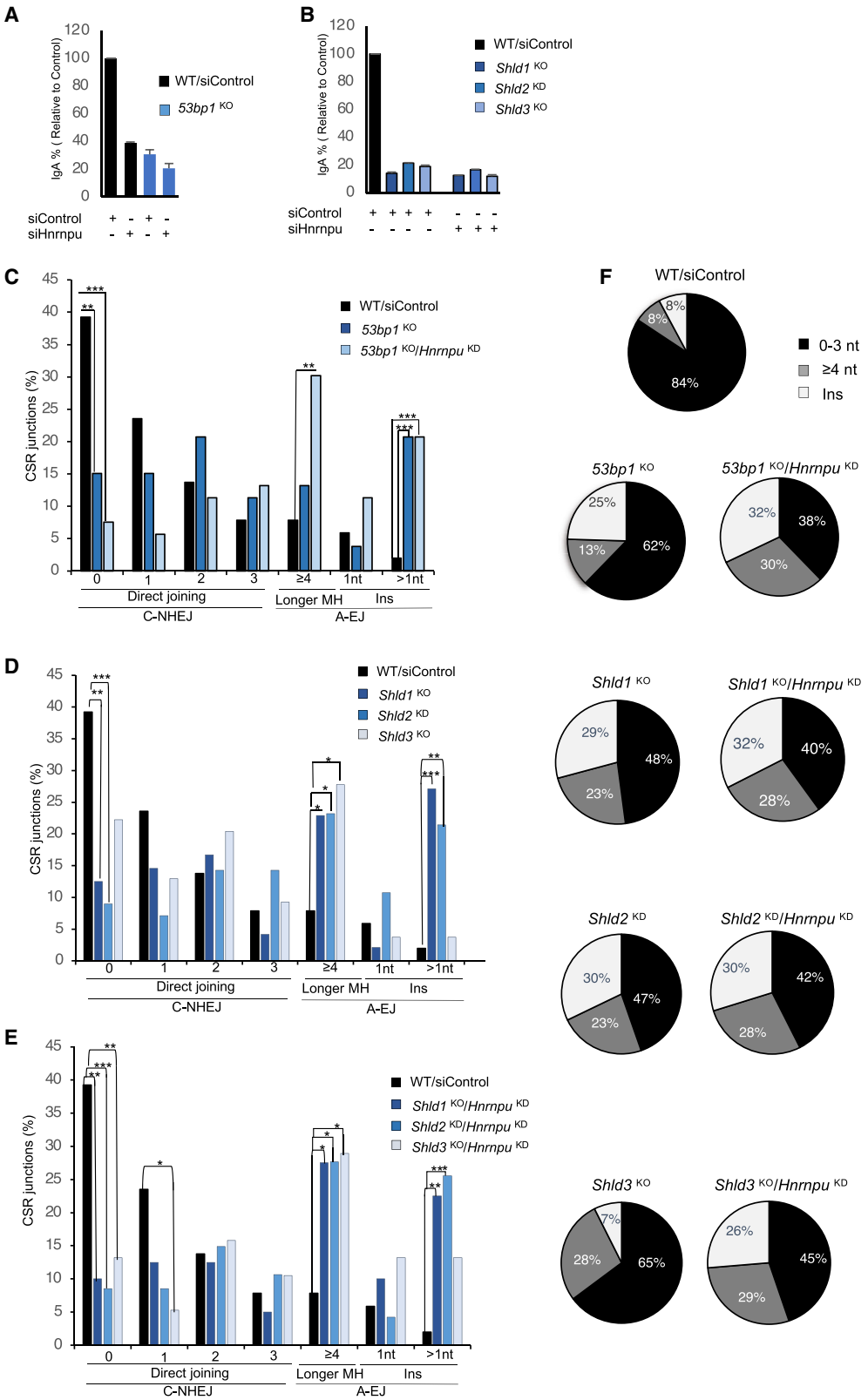

(legend on next page)

a significant increase in longer MH (≥4 nt) usage in *Shld1*^{KO} and *Shld2*^{KD} cells (23%) compared with WT (8%) and similar to *Hnrnpu*^{KD} (28%) (Figures 2D and 2F). Moreover, the CSR junctions of both *Shld1*^{KO} and *Shld2*^{KD} cells showed elevated Ins (29% and 30%), as observed in the *Hnrnpu*^{KD} cells (35%) (Figures 2D and 2F). Consistent with this observation, when *Hnrnpu*^{KD} was combined with *Shld1*^{KO} or *Shld2*^{KD}, CSR junctions did not show any additive influence in direct joining (0–3 nt; 40% and 42%, respectively), longer MH usage (≥4 nt; 28%), or In frequency (Figures 2E and 2F).

Interestingly, 65% of the sequenced CSR junctions in *Shld3*^{KO} cells showed direct joining (0–3 nt), similar to what was observed in *53bp1*^{KO} cells (62%) (Figures 2D and 2F). However, longer MH (≥4 nt) usage in *Shld3*^{KO} cells (28%) was comparable with *Shld1*^{KO}, *Shld2*^{KD}, and *Hnrnpu*^{KD} cells (23%–28%) (Figure 2F). Strikingly, *Shld3*^{KO} cells had CSR junctions with only a few Ins at nearly the same level as those in the WT/siControl-treated cells (Figures 2D and 2F). As expected, when *Hnrnpu*^{KD} was combined with *Shld3* ^{KO}, direct joining was reduced (0–3 nt; 65%–45%), and the In frequency in the double-deficient cells became similar to the *Hnrnpu*^{KD} cells (Figures 2E and 2F). Overall, shieldin-deficient cells, particularly SHLD1 and SHLD2 cells, showed CSR junctional features comparable with those of *Hnrnpu*^{KD} cells, suggesting an overlapping functional pathway in CSR.

HNRNPU is dispensable for SHM but not *IgH/c-Myc* translocation

To better understand the role of HNRNPU in AID-induced Ig gene diversification, we investigated S region hypermutations and *IgH/c-Myc* translocations. Although HNRNPU-depleted cells showed a slight increase in S-SHM frequency, the overall SHM frequencies did not differ significantly among the samples compared with the WT/siControl-treated cells (Figures S3A–S3C; Table S3). No specific base bias was detected in the mutation pattern (Figure S3B). The unaltered mutation frequency in *53bp1* ^{KO} cells agrees with a previous report that 53BP1 is dispensable for S-SHM and V-SHM.[8,44] We therefore conclude that HNRNPU is dispensable for S-SHM during CSR but is essential for S-S recombination.

Next, we examined the CSR-associated *IgH/c-Myc* translocations by analyzing the translocated genomic junctions (Figure S3D). Consistent with CSR impairment in HNRNPU-depleted cells, the *IgH/c-Myc* translocation frequency was significantly reduced (Figures S3E and S3F). Strikingly, the shieldin, but not *53bp1*, deficiency impaired *IgH/c-Myc* translocation, suggesting that HNRNPU and shieldin are functionally interlinked and impact both the *cis* and *trans* recombinational repair required for CSR and *IgH/c-Myc* translocation, respectively. Concerning 53BP1, our data are consistent with the finding that *53bp1* deficiency does not affect or increase AID-induced *IgH/c-Myc* translocation.[45,46] We confirmed that AID-induced DSB frequency did not differ among HNRNPU, 53BP1, or shieldin complex deficiency by linker ligation-mediated PCR (LM-PCR) assay (Figures S3G–S3I), further emphasizing that the role of HNRNPU in DNA repair is similar to that of 53BP1/shieldin.

HNRNPU is associated with the DDR

Because HNRNPU is critical in the DNA-repair phase of CSR, we examined HNRNPU protein expression in response to DNA breaks other than AID-induced damage. We treated 293T cells with increasing doses of etoposide, a potent pharmacological inhibitor of topoisomerase II, which causes genome-wide DSBs and/or DNA damage.[47] As evident in Figure S4A, HNRNPU steadily increased in expression in response to etoposide treatment. Consistent with the notion that etoposide-induced DNA lesions are repaired by C-NHEJ,[47,48] there was a gradual increase in KU80 and 53BP1 (Figure S4A). To test whether HNRNPU interacts with the DDR and C-NHEJ factors in response to DNA damage, we performed HNRNPU immunoprecipitation (IP) in 293T cells exposed to etoposide. A pronounced interaction was observed with γH2AX, KU80, 53BP1, catalytic subunit of the DNA-dependent protein kinase (DNA-PKcs), and FEN1 (Figures S4B and S4C), some of which were enhanced in response to etoposide. Consistently, a notable fraction of etoposide-induced DNA damage foci showed the nuclear co-localization of HNRNPU with γH2AX, KU80, and 53BP1 (Figures S4F–S4K). Interestingly, HNRNPU interacted specifically with structure-specific ssDNA endonuclease FEN1, but not ASTE1, which was recently implicated in the processing of DSB ends with 3′ overhangs.[49,50]

As expected, SHLD1-MF IP by anti-FLAG pulled down the same protein complex, including HNRNPU (Figure S4D). IgG/FLAG IP using non-transfected 293T cells did not pull down any of these proteins (Figures S4B–S4D and S6A). Next, we examined HNRNPU and AID expression during S region DSBs in CH12F3-2A cells in response to CIT. The AID expression corresponded with the DSB marker γH2AX and rapidly peaked within 24 h (Figure S4E). HNRNPU showed mild but sustained increased expression that reached saturation at 48 h. Moreover, increased occupancy of HNRNPU at the recombining S regions was observed in response to CSR activation and AID expression (Figures 1D and 1E), further emphasizing a DNA-damage-response-specific function of HNRNPU in CSR. Overall, our result is also consistent with a previous study that shows rapid recruitment of HNRNPU to radiation-induced DNA damage sites.[51]

HNRNPU facilitates the recruitment of C-NHEJ factors

Because HNRNPU depletion significantly diminished C-NHEJ-mediated S-S recombination, we examined whether the

Figure 2. Pronounced C-NHEJ defect in HNRNPU and 53BP1 double deficiency

(A and B) IgM-to-IgA switching profile of WT, 53BP1, and shieldin KO/KD CH12F3-2A cells transfected with indicated siRNAs (siControl or siHnrnpu). These data are the mean ± SD (n = 3). The percentage of IgA-switched cells was normalized to the value of the WT/siControl samples (=100%).

(C–E) Analyses of junction features of Sμ-Sα recombination in genomic DNA isolated from CH12F3-2A cells stimulated with CIT for 48 h. Comparison of WT vs. *53BP1*^{KO} and siHnrnpu-transfected *53BP1*^{KO} CH12F3-2A cells (C). Comparison of WT vs. *Shld1*^{KO}, *Shld2*^{KD}, and *Shld3*^{KO} CH12F3-2A cells (D). Comparison of WT vs. siHnrnpu-transfected *Shld1*^{KO}, *Shld2*^{KD}, and *Shld3*^{KO} CH12F3-2A cells (E). Statistical significance according to Fisher's exact test is shown. The values are presented as mean ± SD (n = 3).

(F) Pie charts showing the distribution of Sμ-Sα junction features derived from the indicated genomic DNA samples.

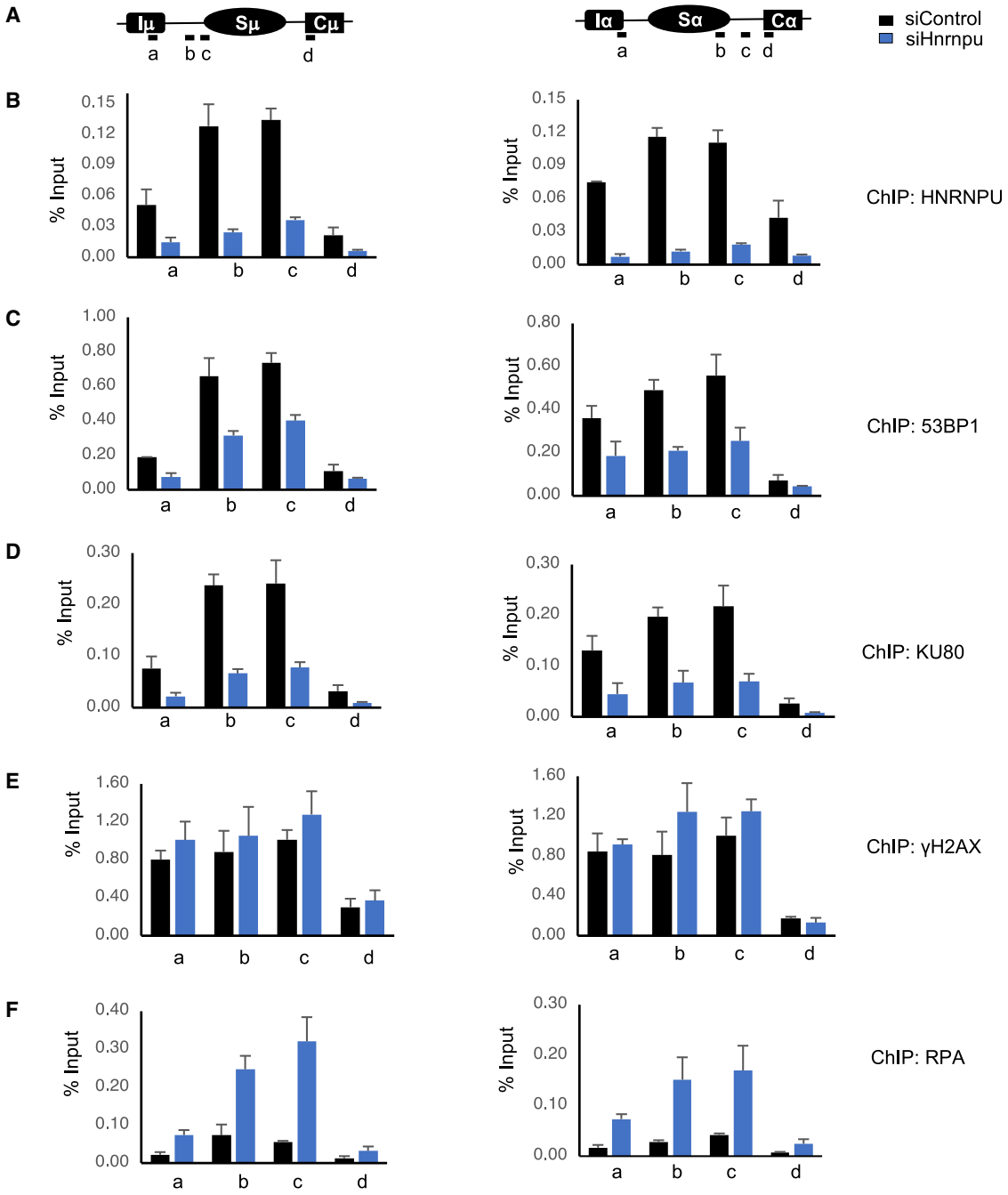

Figure 3. HNRNPU depletion affects DNA-repair factor recruitment

(A) Schematic diagram of the Sμ and Sα regions of the mouse *IgH* locus. The tiny black bars below the scheme indicate the positions (a–d) of the ChIP assay PCR products.

(B–F) ChIP assays using siControl- and siHnrnpu-transfected CH12F3-2A cells stimulated with CIT for 24 h. The antibody used for each ChIP assay is listed on the right-hand side of the respective panel. ChIP data were normalized to the input DNA, and the values are presented as means ± SD (n = 3).

recruitment of critical CSR-repair factors was also affected. The depletion of HNRNPU caused a significant reduction in HNRNPU, 53BP1, and KU80 occupancy at Sμ and Sα (Figures 3A–3D). There was no decrease in DSB-induced γH2AX signal in HNRNPU-depleted cells, confirming an uninterrupted S region DSB (Figure 3E). This result is consistent with the LM-PCR result demonstrating the dispensability of HNRNPU in AID-induced S region DSBs (Figure S3H). Moreover, there was a striking elevation of replication protein A (RPA) in HNRNPU-depleted cells (Figure 3F), similar to 53BP1/shieldin deficiency

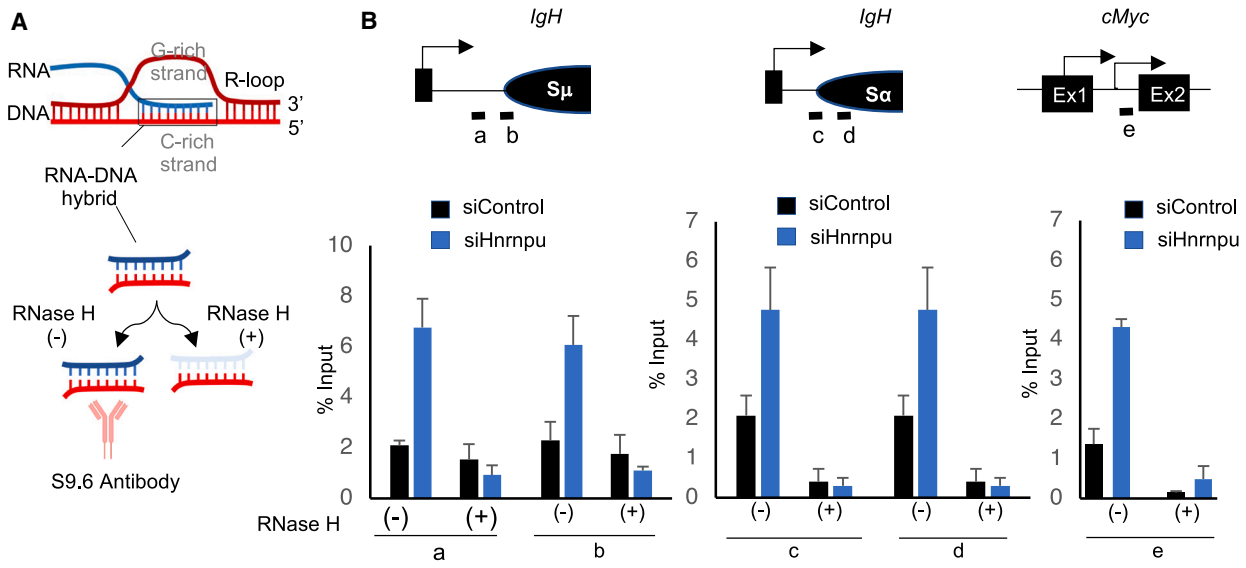

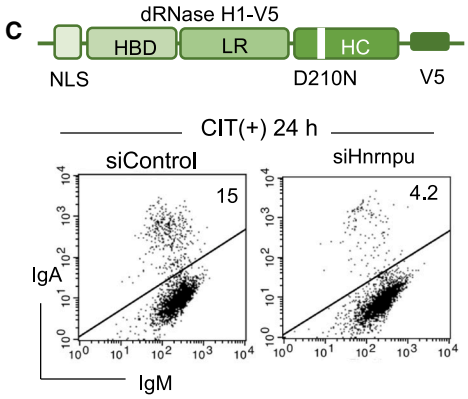

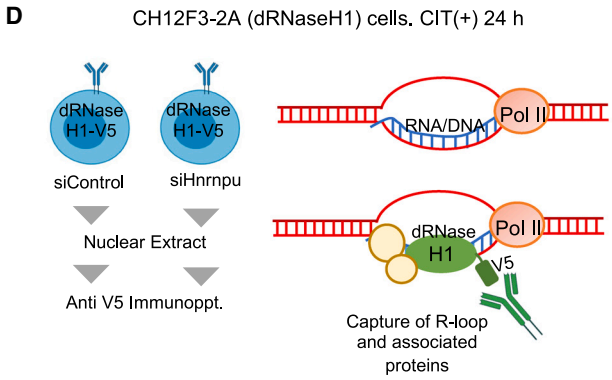

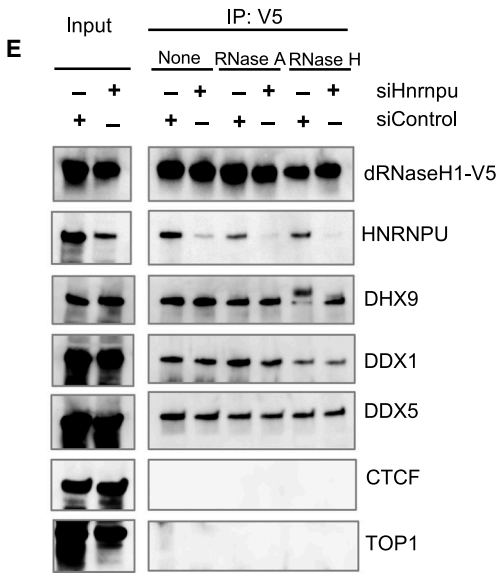

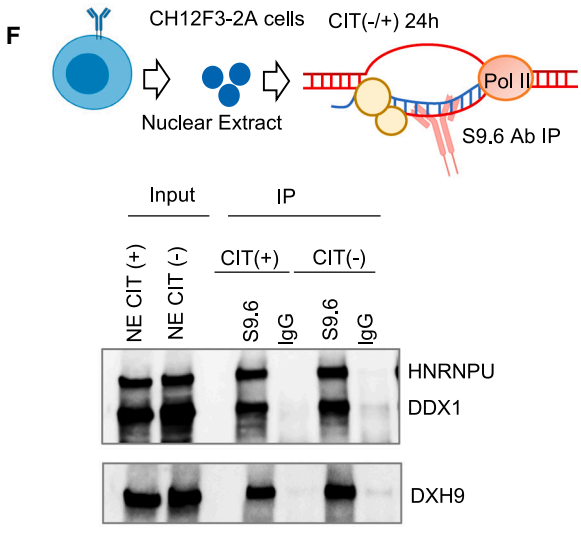

(legend on next page)

caused by excessive DNA end resection and ssDNA accumulation.[13,46] These data suggest that HNRNPU facilitates the stabilization/recruitment of critical DNA-repair factors that regulate DNA end resection at the DSB. This conclusion is further supported by the finding that both HNRNPU and SHLD1 interact with the DNA 5′ flap-end processing enzyme FEN1, and the loss of FEN1 impairs C-NHEJ (Figure S5).[52]

HNRNPU loss increases R-loop and DSB end resection

Because R-loop/DNA:RNA hybrid formation facilitates DNA end resection, which in turn can promote homology-directed repair,[28] we speculated a possible alteration in the S region on HNRNPU depletion. We conducted DNA:RNA IP (DRIP) using an S9.6 antibody that exclusively detects the DNA:RNA hybrid structure in a sequence-independent manner (Figure 4A).[53] HNRNPU depletion resulted in a substantial increase in DNA:RNA hybrid formation at the recombining S regions and at the *c-Myc* locus (Figure 4B). Because elevated R-loop facilitates AID-induced DSB,[31,54] this result is consistent with the persistent γH2AX signal at the S region.

To test whether HNRNPU associates with the R-loop/DNA:RNA hybrid complex, we generated a CH12F3-2A line expressing catalytically dead RNaseH1 (dRNaseH1) with a V5 epitope tag (Figure 4C).[55,56] The CH12F3-2A line expressing dRNaseH1-V5 showed IgA switching and its inhibition on HNRNPU depletion (Figure 4C). As depicted in Figure 4D, we pulled down the DNA:RNA hybrid-specific protein complex by anti-V5 IP of dRNaseH1-V5 from the indicated siRNA-transfected cells stimulated with CIT. The detection of HNRNPU in the R-loop complex was specific, because it corresponded well with HNRNPU protein levels in siControl- or siHnrnpu-treated cells. The presence of three R-loop-associated helicases, DHX9, DDX1, and DDX5, further validated the dRNaseH1-V5-specific pull-down (Figure 4E).[55,57] In addition, we pulled down the R-loop complex by S9.6 IP and reconfirmed the presence of HNRNPU, along with DDX1 and DHX9 (Figure 4F). DNA damage by laser irradiation induces transient R-loops, where co-localization of HNRNPU with other DNA-repair proteins was also observed.[51] Taken together, we conclude that the loss of HNRNPU upregulates S region R-loop and DSB end resection, as evidenced by the enrichment of ssDNA sensor RPA.[58,59]

HNRNPU binds to switch RNA/DNA G4s

Because S regions are enriched with tandem G clusters, the GLTs and the non-template strand are prone to forming G4 structures.[25,60] Because HNRNPU binds telomeric G4 structures,[35] we investigated whether HNRNPU binds to S region G4-RNA/DNA. We used biotinylated synthetic RNA/ssDNA oligonucleotides (b-Oligos) containing four tandem G repeats representing Sμ GLT/non-template strand for a pull-down assay (Figures 5A, S6D, and S6E). More HNRNPU was pulled down with SμG4-RNA folded in the presence of KCl than the LiCl-treated oligo. No binding of HNRNPU was observed with $S\mu G4^{mut}$, a mutated RNA oligo lacking G4-forming potential because of C-substitutions in its tandem G stretches (Figures 5B and S6E). As previously observed, SμG4-RNA, but not the $S\mu G4^{mut}$ RNA, pulled down DDX1 (Figure 5B).[34]

We next tested ssDNA and dsDNA b-Oligos with identical Sμ sequences (Figure S6E). HNRNPU showed a significant binding with SμG4-ssDNA pre-folded in the presence of KCl, but not LiCl. No HNRNPU binding was detected with the SμG4 sequence that formed the dsDNA. DHX36 showed a strong interaction with SμG4-RNA/ssDNA, but not SμG4-dsDNA, which is consistent with its affinity for G-rich RNA/ssDNA. RPA32 binding to SμG4-ssDNA, but not SμG4-dsDNA, is consistent with its specificity for binding to ssDNA and the S region (Figure 5C).[61] We also pulled down AID with the KCl-folded SμG4-RNA/ssDNA to confirm the validity of the assay (Figure 5D).[60] The slot blot (SB) assay panels (Figures 5B–5D) confirmed that the RNA/DNA amounts recovered from streptavidin beads under different conditions were comparable.

The binding of HNRNPU to telomeric G4 DNA has been shown to be dependent on its C-terminal arginine/glycine-rich (RGG) domain.[35] In order to examine the requirement of the RGG domain for binding SμG4-RNA/ssDNA, we conducted another binding assay using HNRNPU protein. We expressed WT and RGG domain-deleted HNRNPU in 293T cells and used FLAG-IP (Figures 5E–5G). Consistent with the result of CSR-activated B cells (Figures 5B and 5C), ectopically expressed WT HNRNPU showed a similar binding affinity with SμG4-RNA/ssDNA pre-folded in KCl buffer (Figures 5F–5H). Surprisingly, RGG-domain-deleted HNRNPU (ΔRGG) could not bind effectively to SμG4-RNA/ssDNA (Figure 5H). Conversely, the RGG domain itself showed binding with SμG4-RNA/ssDNA was comparable with WT (Figure 5H), suggesting the C terminus of HNRNPU is crucial for recognizing both RNA and ssDNA G4s present in the S region. In other words, HNRNPU can bind the G4 structure of GLTs and the non-template ssDNA in the S region and/or R-loop.[62]

Figure 4. HNRNPU depletion increases R-loop at *IgH* and *c-Myc* loci

(A) Schematic depiction of the R-loop/DNA:RNA hybrid after immunoprecipitation with an S9.6 antibody (DRIP assay) with and without RNaseH treatment.

(B) Top: schematic representation of *IgH* locus Sμ and Sα regions and the *c-Myc* locus. Small black bars are the positions of the DRIP-qPCR products. Bottom: R-loops were quantified by DRIP-qPCR at the indicated positions in the *IgH* and *c-Myc* loci. The DRIP-qPCR results show the levels of DNA enriched at the indicated sites relative to the input. The values are presented as means ± SD (n = 3).

(C) Top: schematic diagram of the dRNaseH1-V5 construct introduced into CH12F3-2A cells. Bottom: a representative FACS profile of IgM-to-IgA switching in siControl- or siHnrnpu-treated CH12F3-2A cell lines expressing dRNaseH1-V5.

(D) An illustration depicting the indirect capture of the R-loop/DNA:RNA hybrid complex.

(E) Anti-V5 antibody immunoprecipitation of the dRNaseH1-V5-bound complex and detection of the indicated coimmunoprecipitated proteins by immunoblot analysis.

(F) Top: workflow of the direct capture of the R-loop/DNA:RNA hybrid complex by S9.6 antibody immunoprecipitation. Bottom: detection of HNRNPU, DDX1, and DHX9 in the DNA:RNA hybrid complex pulled down by S9.6 antibody immunoprecipitation.

D210N, catalytic inactivation mutation; HBD, DNA:RNA hybrid binding domain; HC, DNA:RNA hybrid catalytic domain; LR, linker region; NLS, nuclear localization signal; V5, V5 epitope tag.

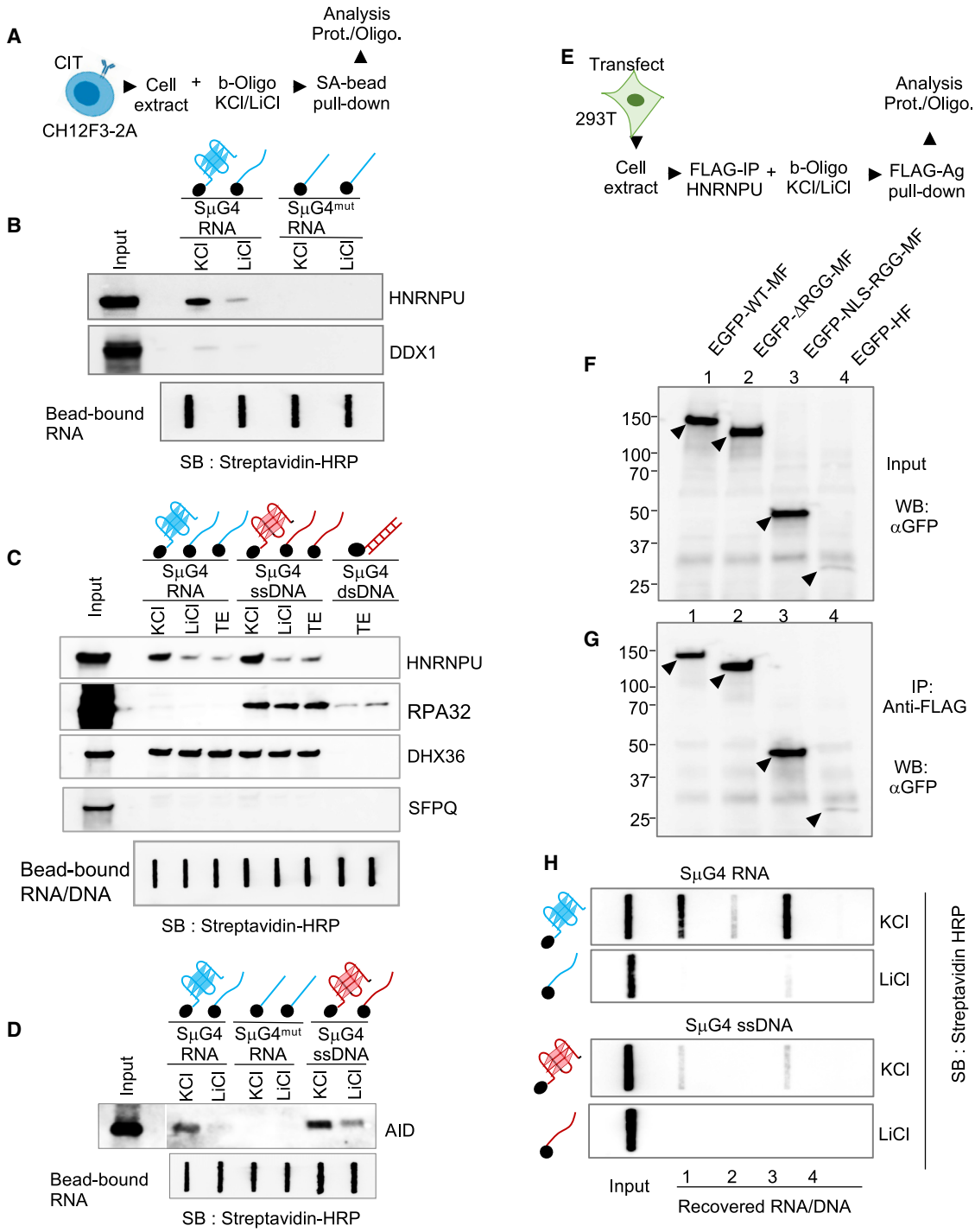

Figure 5. HNRNPU binds to Sμ G-quadruplex (G4)

(A) Biotinylated oligonucleotide (b-Oligo) pull-down assay using CH12F3-2A cells.

(B) Western blot analysis of proteins (HNRNPU and DDX1) pulled down by b-RNA-Oligo, SμG4, and SμG4^{mut} (for sequences, see Figure S6E). The G4 and the linear structure produced in different buffers are indicated on the top. Slot blot (SB) analysis shows the streptavidin (SA) magnetic-bead-bound input b-RNA-Oligos.

(C) Western blot and SB analyses of the pull-down assay using b-RNA/b-ssDNA/b-dsDNA Oligo of identical SμG4 sequence. RPA32 was used as a control for ssDNA-binding protein. None of the conditions showed SFPQ binding to SμG4 sequences, thus serving as an excellent negative control.

(D) AID was examined as a positive control for Sμ-derived G4 RNA/ssDNA.

(legend continued on next page)

HNRNPU interacts with C-NHEJ and R-loop complex

Because HNRNPU is involved in both C-NHEJ and R-loop regulation, we performed HNRNPU IP using nuclear extracts from CIT-stimulated CH12F3-2A cells in the absence (−) or presence (+) of RNase A (Figure 6A). In this assay, HNRNPU interacted with well-known and recently identified C-NHEJ factors, including KU80, DNA-PKcs, and SFPQ. As expected, the HNRNPU complex also contained R-loop/DNA:RNA hybrid-associated proteins DHX9, DDX1, TOP1, NONO, and SFPQ (Figure 6A). This result is consistent with the identification of HNRNPU in the R-loop complex by S9.6 and dRNaseH1-V5 IP (Figure 4).

Because CSR junctions in the context of HNRNPU deficiency are highly similar to shieldin deficiency, especially with SHLD1, we speculated that HNRNPU and SHLD1 might interact and/or share the same protein complex. Therefore, we performed SHLD1 IP, as a representative of the shieldin and C-NHEJ complex, from nuclear extract of transfected CH12F3-2A cells (Figure 6B). Normal IgG and an FLAG IP of untransfected CH12F3-2A cells served as negative controls (Figures 6B and S6C). Indeed, SHLD1 IP pulled down HNRNPU, along with KU80, DNA-PKcs, and 53BP1, which are expected to associate with the shieldin/C-NHEJ complex. Strikingly, SHLD1 IP also pulled down several R-loop-associated proteins (DDX1, DHX9, SFPQ, NONO, and FEN1) that coimmunoprecipitated with HNRNPU (Figure 6B). We reproduced the interaction between SHLD1 and HNRNPU, KU80, and FEN1 in 293T cells (Figure S7B), further supporting HNRNPU's association with the C-NHEJ complex in non-B cells.

Notably, many of these interactions with HNRNPU were highly sensitive to RNase A treatment (Figure 6A), suggesting that HNRNPU likely forms a ribonucleoprotein complex with C-NHEJ and R-loop-associated cofactors. HNRNPU without the RGG domain failed to interact with KU80, SFPQ, NONO, or TOP1 but retained a substantial interaction with FEN1 (Figure S7A), suggesting that the HNRNPU complex contains both protein-protein and RNA-protein interacting partners. A complementary IP using selected HNRNPU interacting proteins successfully pulled down HNRNPU with all its interacting partners (Figures S7C–S7H). Benzonase treatment, which degrades RNA and DNA, showed a similar result as observed with RNase A treatment (Figure 6A), suggesting that most interactions were RNA mediated. Notably, the HNRNPU and FEN1 interaction turned out to be a protein-protein interaction.

Next, we examined whether the complex contains the C-NHEJ-associated long noncoding RNA *LINP1*, which tethers DNA-PKcs and KU70/80 to promote C-NHEJ.[63,64] We isolated HNRNPU- or SHLD1-bound RNA using 293T cells transfected with FLAG-tagged HNRNPU or SHLD1. The successful capture of the FLAG-tagged bait proteins and their interaction with KU80 were confirmed in their respective IP complexes (Figure 6C). Quantitative RT-PCR showed significant enrichment of *LINP1* RNA in the complex pulled down by HNRNPU or SHLD1, but not IgG (Figure 6C). The lack of enrichment of unrelated *GAPDH* RNA confirms the specificity of the IP. The presence of a comparable amount of *LINP1* with HNRNPU and SHLD1 further emphasizes their physical and functional link with the C-NHEJ complex (Figure 6D).

HNRNPU harbors intrinsically disordered regions (IDRs) and is functionally perturbed by liquid-liquid phase separation (LLPS) inhibitors

An increasing number of studies suggest that proteins with IDRs are involved in DDR and repair.[65–67] The IDR domains in the proteins drive LLPS or condensation to form specialized compartments or condense to facilitate DSB/DNA damage repair.[68,69] Specific noncoding RNAs are often the principal driving force for sequestering the phase separation and are thus sensitive to chemical agents and environmental alterations that disrupt the LLPS.

Sequence analysis of HNRNPU predicted that it contains IDRs at the N and C termini (Figure 7A). Intriguingly, the C-terminal IDR extended over the RGG domain, which appears crucial for RNA-dependent DNA-repair complex formation (Figures 6A and S7A). We performed a protein precipitation assay (Figure S8A) using biotinylated isoxazole (b-isox), a chemical known to selectively precipitate IDR-containing proteins from cell-free lysates.[70] In this assay, b-isox precipitated HNRNPU in a dose-dependent manner from both unstimulated and CIT-stimulated CH12F3-2A cell extracts (Figure 7B). AID was precipitated from CIT-activated cell lysates but to a lesser extent than HNRNPU, consistent with a recent report that AID has a weak IDR.[71] To confirm further, we used 293T cells to ectopically express WT and mutant HNRNPUs (Figures S8A and S8B). Endogenous HNRNPU and EGFP and FLAG epitope-tagged WT HNRNPU were readily detected in the b-isox precipitate compared with RGG domain-deleted HNRNPU (Figure S8C). In contrast, the RGG domain alone (with or without NLS) was present in the b-isox precipitate similar to WT (Figure S8D), suggesting the RGG domain embedded within the C-terminal IDR contributes significantly.

Next, we treated CH12F3-2A cells with 1,6-hexanediol (1,6-HD) or ammonium acetate (NH4OAc), which disrupt LLPS or condensate formation *in vivo* by perturbing multivalent hydrophobic protein-protein and/or RNA-protein interactions.[72–74] We used the lowest dose that effectively inhibited CSR while also not affecting cell proliferation or GLT and AID transcription. The treatment of CH12F3-2A cells with 1,6-HD or NH4Ac drastically reduced HNRNPU occupancy at the S regions, accompanied by the loss of 53BP1 and KU80 (Figures 7C and 7D, upper panel). We confirmed that the expression levels of HNRNPU, 53BP1, and KU80 proteins were not affected by the LLPS inhibitors (Figure S8E). Intriguingly, the accumulation of DSB-induced H2AX and RPA phosphorylation and R-loop-associated H3S10 phosphorylation remained unchanged

(E) Assay of b-Oligo binding to HNRNPU using 293T cells.
(F and G) Representative western blots showing the expression levels and successful FLAG-IP of the indicated constructs.
(H) SB analysis of b-RNA/b-ssDNA Oligo recovered from FLAG-agarose-bound WT or mutant HNRNPU.
Data shown in (B)–(D) and (F)–(H) are representative of more than three experiments. FLAG-Ag, anti-FLAG-conjugated agarose bead; HF, HA-FLAG; MF, Myc-FLAG; SA-Bead, streptavidin magnetic bead.

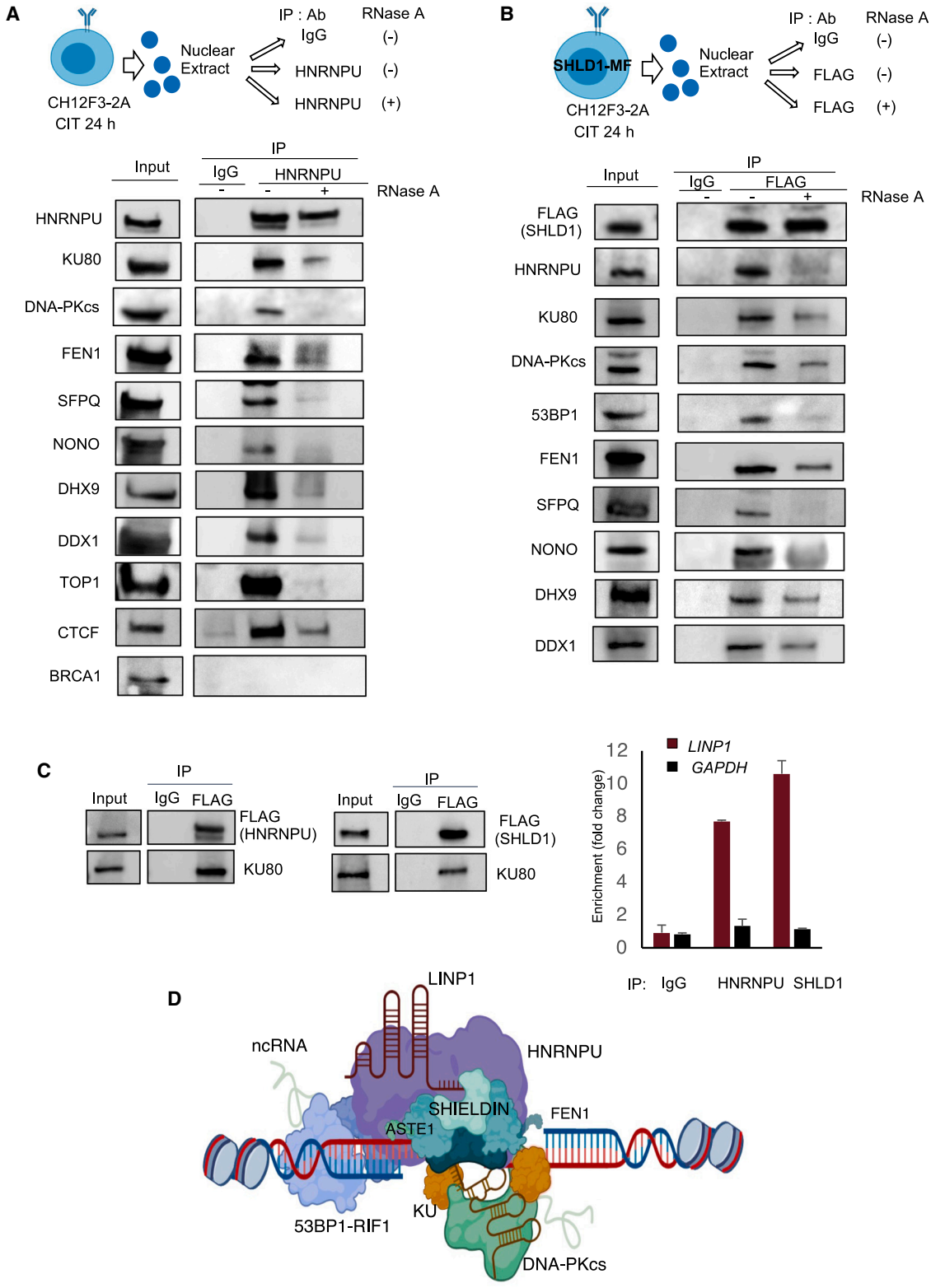

Figure 6. HNRNPU associates with C-NHEJ and R-loop complex

(A) Endogenous HNRNPU was immunoprecipitated from the nuclear extracts of stimulated CH12F3-2A cells with and without RNase A treatment. The HNRNPU IP complex was subjected to a series of immunoblot analyses as indicated.

(legend continued on next page)

(Figure 7D, lower panel), suggesting that NHEJ-complex formation was particularly affected. In contrast, treatment with RNAP II inhibitor α-amanitin/DRB abolished all signals, indicating that transcription and/or RNAs are upstream of both DNA break and repair sites. These results suggest that the DNA-repair complex assembly at the S region requires LLPS and condensate formation involving HNRNPU and the C-NHEJ factors necessary for CSR.

DISCUSSION

HNRNPU promotes CSR by facilitating C-NHEJ-mediated DNA repair

AID-induced S region DSBs are repaired primarily by the C-NHEJ pathway, which involves no or short MH (1- to 3-nt)-dependent DSB joining. In the absence of C-NHEJ, CSR junctions are repaired via A-EJ using longer MHs (≥4 nt) and insertional DNA repair, which reduces CSR efficiency.[16,41,75] In HNRNPU deficiency, the Sμ-Sα recombination junctions showed a sharp drop in direct or blunt-end joining (3.9-fold) and an elevation in longer MHs (≥4 nt; 3.5-fold) and Ins (4.3-fold) at the recombination junctions. This finding is consistent with the C-NHEJ defect on HNRNPU depletion, which is usually compensated for by the backup A-EJ pathway, as observed in well-known C-NHEJ factor deficiencies, such as KU70/80, XRCC4, LIG4, and DNA-PKcs.[76] SHLD1 or SHLD2 deficiency reduced the C-NHEJ signature and increased the frequencies of longer MHs and Ins at the CSR junctions (Figures 2D and 2F; Tables S1 and S2). In contrast, SHLD3 and 53BP1 depletion induced a modest decrease in the C-NHEJ signature and an increase in longer MHs. Consistent with a previous report,[44] 53BP1 deficiency led to increased Ins, whereas SHLD3 deficiency was completely devoid of any Ins at the CSR junctions, which may reflect unrecognized functional differences among the shieldin subunits. Overall, this comparison study suggests that the CSR DNA-repair regulation by HNRNPU has a high similarity with SHLD1/2-dependent C-NHEJ. HNRNPU depletion in combination with SHLD1/2 did not have an additive impact on C-NHEJ-mediated repair of CSR junctions (Figures 2E and 2F), implicating impaired SHLD1/2 function was likely responsible for the C-NHEJ defect observed in HNRNPU deficiency. Because the shieldin complex binds directly to ssDNA through SHLD2 at the DSB site, in its absence, RPA occupies the exposed ssDNA.[13] Notably, HNRNPU deficiency exhibited the same feature, a striking increase in RPA occupancy at the S regions (Figure 3F), suggesting that HNRNPU loss causes excessive ssDNA formation and fails to recruit shieldin and other essential C-NHEJ factors.

Recently, it has been shown that ASTE1, an XPG family 3′ DNA endonuclease, directly interacts with SHLD2 and facilitates the processing of DSB ends with 3′ overhangs. Our study shows that another XPG family nuclease, FEN1, with 5′ flap endonuclease and 5′–3′ exonuclease activities, not only interacts with HNRNPU but also with SHLD1, and its depletion impairs IgA switching in CH12F3-2A cells (Figure S5). CSR junction analysis of FEN1-deficient CH12F3-2A cells also showed a typical defect of C-NHEJ with a decrease in direct joining and elevation of longer MHs and Ins, which corresponded to HNRNPU and shieldin deficiency (Figure S5). Therefore, ASTE1 and FEN1, associated with SHLD2 and SHLD1, respectively, can facilitate ssDNA overhang processing at S region DSBs to promote DNA repair through C-NHEJ. In agreement with the requirement of NHEJ for chromosomal translocations,[77,78] SHLD1/2 and HNRNPU deficiencies significantly decreased AID-induced *IgH/c-Myc* translocations.

HNRNPU forms an RNA-dependent C-NHEJ complex

In B cells stimulated for CSR, the recruitment of HNRNPU at the recombining S regions was strikingly elevated, suggesting its intimate connection with AID-induced DNA damage and repair. In line with this, the loss of HNRNPU reduced the recruitment of 53BP1 and KU80 at the S regions, resulting in inefficient C-NHEJ-mediated repair of the CSR junctions.

Consistent with HNRNPU's involvement with the DNA-repair phase of CSR, HNRNPU interacted with KU80, DNA-PKcs, 53BP1, and the shieldin complex, which are essential C-NHEJ factors in CSR. In addition, the HNRNPU complex also contains the SFPQ-NONO heterodimer (Figure 6A), which binds with KU proteins and functions at the ligation step of C-NHEJ.[79,80] Britton et al.[51] also showed that HNRNPU interacts with SFPQ through its RNA-binding RGG domain. Intriguingly, our study also indicates that the interaction between HNRNPU and the NHEJ factors is RGG domain dependent and thus sensitive to RNase A treatment (Figures 6A and S7A).

As such, it is highly conceivable that RNA-mediated C-NHEJ complex formation occurs during CSR DNA repair. It is known that 53BP1 binds to RNA- and DNA-damage-induced noncoding RNAs, which is functionally relevant because 53BP1 foci formation at the DNA damage site is impaired by RNase A treatment.[22,81] Similarly, the RNA-binding property of KU and DNA-PKcs is critical for their function in C-NHEJ.[82,83] An especially relevant long noncoding RNA is *LINP1*, which stabilizes KU80 and DNA-PKcs at the C-NHEJ synaptic complex.[64] Thus, HNRNPU forms an RNA-dependent C-NHEJ complex or HNRNPU and SHLD1 associate with *LINP1* is highly relevant and in line with the increasing number of studies supporting the involvement of RNA and RBDs in DNA repair.[84,85] In the absence of HNRNPU, increased export of noncoding RNAs from the nucleus was observed because of the lack of their stabilization through HNRNPU.[86] HNRNPU contributes to chromatin organization through its interaction with chromatin-associated noncoding RNAs.[87,88] In this study, HNRNPU can recruit scaffolding noncoding RNAs and other proteins to the *IgH* locus to promote DNA-repair factor assembly (Figure 6D).

(B) Ectopically expressed SHLD1-MF IP with an anti-FLAG antibody. The immunoprecipitated SHLD1 complex was subjected to a series of immunoblot analyses as indicated.

(C) Left: confirmation of HNRNPU and SHLD1 pull-down by anti-FLAG IP. Right: qRT-PCR results showing the relative abundance of *LINP1* and *GAPDH* (control) RNA in the HNRNPU or SHLD1 IP. The enrichment was normalized to the input RNA. The values are presented as means ± SD (n = 3).

(D) A model showing the interaction between HNRNPU and the CSR-associated C-NHEJ complex along with the long noncoding RNA *LINP1*.

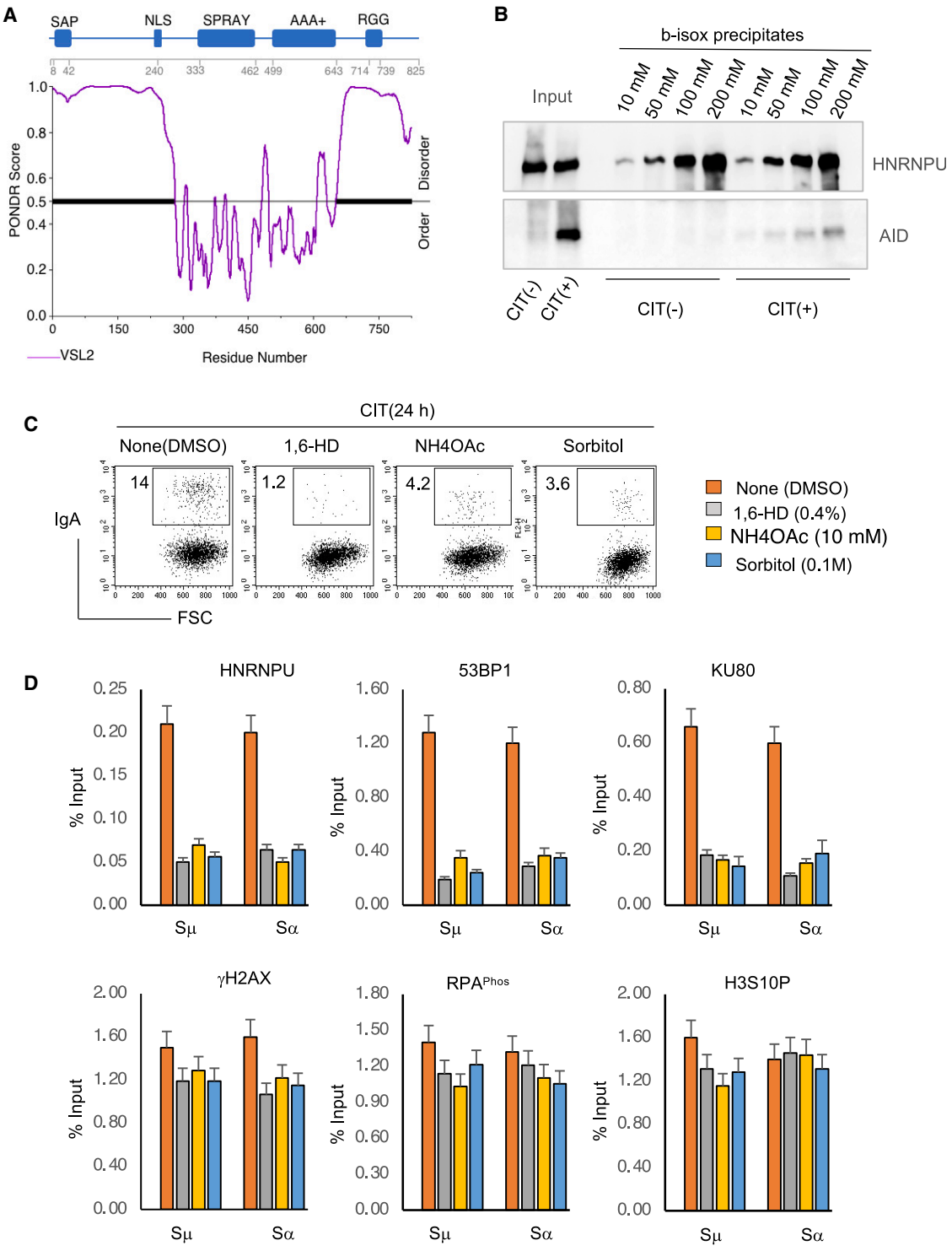

Figure 7. Liquid-liquid phase separation (LLPS) inhibitors disrupt HNRNPU and repair factor recruitment

(A) PONDR prediction of the intrinsically disordered region (IDR) in HNRNPU.

(B) Representative western blots of biotinylated isoxazole (b-isox) precipitation assay using CH12F3-2A cell extracts.

(C) Representative FACS profiles showing the substantial CSR impairment by LLPS-perturbing compounds.

(D) ChIP analyses showing the occupancy of HNRNPU and other DDR factors at S regions in response to indicated LLPS inhibitors. Data were compiled from two independent experiments.

LLPS underlies HNRNPU and C-NHEJ factor recruitment to the S region

RNA-dependent DNA-repair complex formation gains further supportas the accumulation of HNRNPU and NHEJ factors such as 53BP1, upstream of the shieldin complex at AID-induced DSB sites, is sensitive to transcriptional inhibition and LLPS-perturbing agents (Figure 7D). HNRNPU also exhibited characteristics typical of intrinsically disordered proteins along with the RGG domain (Figure 7A) and undergoes oligomerization in an ATP- and RNA-dependent manner.[87,89] An earlier study also showed that the C-terminal low-complexity RNA-binding region has the feature of a prion-like domain (PLD) that forms a polymer-like "mesh" structure linking RNA and DNA.[90,91]

Several RBDs, including FET proteins (FUS, TAF15, and EWSR1) and RBM14, possess IDRs and PLDs, which are recruited to the DNA damage site where PAR formation and LLPS occur.[65,92,93] HNRNPU has also been shown to bind PAR and be recruited to the laser-induced damage site in a PAR-dependent manner through its C terminus.[51] High local concentrations of specific RNA and PAR formation at the DNA damage site act as a seed for condensation by promoting multivalent RNA-protein and/or protein-protein non-covalent interactions. Our study shows that a 40-nt sequence from the S region RNA/DNA, when folded into G4 structure, binds more HNRNPU as reported for telomeric G4-repeat structure. Because repetitive and G4 RNAs can promote LLPS,[94] S-GLTs and/or G4-structured RNAs could be involved in HNRNPU-associated condensate formation during CSR. The interaction of HNRNPU with repetitive, repeated domain RNA significantly impacts genomic architecture, and thus its loss or failure to oligomerize can trigger chromosomal instability.[87–89] The DDR factor 53BP1 also contains IDR and RGG-like domains at the C terminus and undergoes RNA-dependent oligomerization.[67] Intriguingly, 53BP1 recruitment to the S region, in response to AID-induced DSB, can be entirely disrupted by LLPS-perturbing chemicals 1,6-HD and NH4OAc and conditions such as sorbitol-induced osmotic dysregulation,[66,67] suggesting that CSR recombination/repair foci involve nuclear condensate formation.

HNRNPU prevents R-loop and DNA end resection

Bidirectional transcription through GC-rich, repetitive S regions promotes R-loop formation and induces ssDNA on both strands, resulting in non-B structures and AID-induced DNA breaks.[32] GLT processing and post-translational modification affect R-loop and AID targeting, leading to altered DNA break and MH-mediated repair.[30,31,34] In the case of HNRNPU loss, AID-induced DSBs were not affected, as evidenced by the LM-PCR assay and γH2AX occupancy at the S region (Figures 3E and S3H), implying that AID targeting remained intact. Loss of HNRNPU caused a marked decrease in C-NHEJ with a concomitant elevation in MH, as observed because of the DSB-end protection defect in KU80, 53BP1, or shieldin deficiency.

HNRNPU also prevented the accumulation of R-loop and ssDNA at the S region (Figures 3F and 4), facilitating C-NHEJ. Persistent R-loops are roadblocks for efficient repair by C-NHEJ, and nick in the displaced strand of the R-loop generates free ssDNA end, promoting HR.[26,29] Because HNRNPU facilitates DNA-G4 formation, the free ssDNA at the CSR-DSBs may adopt a G4 structure similar to the telomere. HNRNPU resides at the telomere with DNA-PKcs and shelterin complex and contributes to long G-rich ssDNA protection, including telomeric-G4 regulation.[35,95] Intriguingly, HNRNPU binds to the S region G4 through its RGG domain, as in the case of the telomere. Notably, G4-interacting proteins such as FEN1, EXO1, BLM, and 53BP1 interacting protein RIF1 can be found in the CSR-repair complex. RIF1 may favor NHEJ; however, its oligomerization with multiple G4 structures can especially promote CSR, because the S region harbors long stretches of G4.[96,97] Interestingly, DNA-G4 structures have also been reported to promote specific DNA-repair pathways and to facilitate recombination by DNA strand pairing.[98–100] The HNRNPU binding to GLT/G4 (Figures S9 and 5) may regulate the R-loop formation as binding of RBPs to the nascent transcript prevents snap-backing to the template strand, reducing the R-loop.[101] The RNA secondary structure also impacts the R-loop because the G4-structure unwinding by helicase elevates R-loop.[34]

We propose a dual function of HNRNPU in the DNA-repair phase of CSR (Figure S10). First, in response to AID-induced DSBs, elevated HNRNPU at the S regions promotes stabilization of the C-NHEJ complex through a noncoding RNA scaffold. Second, it limits the DNA end-resection/ssDNA accumulation through R-loop and/or DNA-G4 regulation. Identifying noncoding/G4 RNAs involved may reveal how LLPS occurs and how the HNRNPU/C-NHEJ complex promotes S-S recombination. Dynamic compartmentalization by liquid demixing likely occurs to form DNA-repair/recombination-specific condensate formation during CSR.

Limitations of the study

We could not generate *Hnrnpu*^{KO} CH12F3-2A cells by CRISPR-Cas9 targeting due to poor viability. We also faced difficulty in overexpressing HNRNPU in B cells, potentially limiting further functional investigation in B cells. The shieldin antibodies reported are suitable for IP of human, but not mouse, endogenous SHLD proteins, which could help generate additional information on CSR and the role of HNRNPU.

STAR★METHODS

Detailed methods are provided in the online version of this paper and include the following:

- KEY RESOURCES TABLE
- RESOURCE AVAILABILITY
  - Lead contact
  - Materials availability
  - Data and code availability
- EXPERIMENTAL MODEL AND SUBJECT DETAILS
  - Cell lines
  - Mice
  - Primary B-cells
- METHOD DETAILS
  - Gene knockdown transfection
  - Generation and use of stable CH12 lines
  - Constructs and mutagenesis
  - CSR assay in CH12 and primary B cells

- Immunoprecipitation and immunoblotting
- Isolation of HNRNPU- or SHLD1-bound RNA and RT–qPCR
- Class-switch recombination junction analysis
- Analysis of S-region SHM
- *IgH/c-Myc* chromosomal translocation analysis
- RNA extraction, cDNA synthesis, and quantitative RT–PCR
- Double-strand DNA break detection by LM-PCR
- Chromatin immunoprecipitation (ChIP) assay
- DNA–RNA immunoprecipitation (DRIP)
- Immunofluorescence (IF) staining
- Biotinylated SμG4 RNA/DNA oligonucleotide pull-down assay
- Biotinylated isoxazole-mediated HNRNPU precipitation assay

● QUANTIFICATION AND STATISTICAL ANALYSIS

SUPPLEMENTAL INFORMATION

Supplemental information can be found online at https://doi.org/10.1016/j.celrep.2023.112284.

ACKNOWLEDGMENTS

We are thankful to Dr. Andre Stanlie and Dr. Andre Nussenzweig for providing the *53bp1*^{KO}, *Shld1*^{KO}, and *Shld3*^{KO} cell lines. This work was supported by funding from the Japan Society for the Promotion of Science; Grant-in-Aid for Scientific Research (S) 19H01027 and 22H00449 (to T.H.) and Grant-in-Aid for Scientific Research (C) 21K06015 (to N.A.B.). A.M.R. was supported by an Egyptian Japanese Education Partnership PhD scholarship from the Ministry of Higher Education of the Arab Republic of Egypt.

AUTHOR CONTRIBUTIONS

A.M.R. conducted the majority of experimental work and composed the original draft of the manuscript. N.A.B. and M.N. contributed by performing critical experiments. M.N. also facilitated the experiments by providing technical support and preparing essential reagents. A.H. optimized the DRIP assay and provided helpful feedback on the manuscript. H.K. provided valuable assistance in the mass spectrometric (MS) analysis of HNRNPU and the S9.6 immunoprecipitated complex. N.A.B. designed the experiments and wrote and reviewed the manuscript with input from A.M.R. and the co-authors. The project's conceptualization and supervision were under the purview of T.H. and N.A.B.

DECLARATION OF INTERESTS

The authors declare no competing interests.

INCLUSION AND DIVERSITY

We support inclusive, diverse, and equitable conduct of the research.

Received: April 7, 2022
Revised: October 23, 2022
Accepted: March 3, 2023
Published: March 20, 2023

REFERENCES

1. Muramatsu, M., Kinoshita, K., Fagarasan, S., Yamada, S., Shinkai, Y., and Honjo, T. (2000). Class switch recombination and hypermutation require activation-induced cytidine deaminase (AID), a potential RNA editing enzyme. Cell *102*, 553–563. https://doi.org/10.1016/s0092-8674(00)00078-7.
2. Revy, P., Muto, T., Levy, Y., Geissmann, F., Plebani, A., Sanal, O., Catalan, N., Forveille, M., Dufourcq-Labelouse, R., Gennery, A., et al. (2000). Activation-induced cytidine deaminase (AID) deficiency causes the autosomal recessive form of the Hyper-IgM syndrome (HIGM2). Cell *102*, 565–575. https://doi.org/10.1016/s0092-8674(00)00079-9.
3. Chaudhuri, J., and Alt, F.W. (2004). Class-switch recombination: interplay of transcription, DNA deamination and DNA repair. Nat. Rev. Immunol. *4*, 541–552. https://doi.org/10.1038/nri1395.
4. Honjo, T., Kinoshita, K., and Muramatsu, M. (2002). Molecular mechanism of class switch recombination: linkage with somatic hypermutation. Annu. Rev. Immunol. *20*, 165–196. https://doi.org/10.1146/annurev.immunol.20.090501.112049.
5. Lieber, M.R. (2010). The mechanism of double-strand DNA break repair by the nonhomologous DNA end-joining pathway. Annu. Rev. Biochem. *79*, 181–211. https://doi.org/10.1146/annurev.biochem.052308.093131.
6. Rooney, S., Chaudhuri, J., and Alt, F.W. (2004). The role of the non-homologous end-joining pathway in lymphocyte development. Immunol. Rev. *200*, 115–131. https://doi.org/10.1111/j.0105-2896.2004.00165.x.
7. Casellas, R., Nussenzweig, A., Wuerffel, R., Pelanda, R., Reichlin, A., Suh, H., Qin, X.F., Besmer, E., Kenter, A., Rajewsky, K., and Nussenzweig, M.C. (1998). Ku80 is required for immunoglobulin isotype switching. EMBO J. *17*, 2404–2411. https://doi.org/10.1093/emboj/17.8.2404.
8. Manis, J.P., Morales, J.C., Xia, Z., Kutok, J.L., Alt, F.W., and Carpenter, P.B. (2004). 53BP1 links DNA damage-response pathways to immunoglobulin heavy chain class-switch recombination. Nat. Immunol. *5*, 481–487. https://doi.org/10.1038/ni1067.
9. Pan-Hammarström, Q., Jones, A.M., Lähdesmäki, A., Zhou, W., Gatti, R.A., Hammarström, L., Gennery, A.R., and Ehrenstein, M.R. (2005). Impact of DNA ligase IV on nonhomologous end joining pathways during class switch recombination in human cells. J. Exp. Med. *201*, 189–194. https://doi.org/10.1084/jem.20040772.
10. Soulas-Sprauel, P., Le Guyader, G., Rivera-Munoz, P., Abramowski, V., Olivier-Martin, C., Goujet-Zalc, C., Charneau, P., and de Villartay, J.P. (2007). Role for DNA repair factor XRCC4 in immunoglobulin class switch recombination. J. Exp. Med. *204*, 1717–1727. https://doi.org/10.1084/jem.20070255.
11. Setiaputra, D., and Durocher, D. (2019). Shieldin - the protector of DNA ends. EMBO Rep. *20*, e47560. https://doi.org/10.15252/embr.201847560.
12. Di Virgilio, M., Callen, E., Yamane, A., Zhang, W., Jankovic, M., Gitlin, A.D., Feldhahn, N., Resch, W., Oliveira, T.Y., Chait, B.T., et al. (2013). Rif1 prevents resection of DNA breaks and promotes immunoglobulin class switching. Science *339*, 711–715. https://doi.org/10.1126/science.1230624.
13. Ghezraoui, H., Oliveira, C., Becker, J.R., Bilham, K., Moralli, D., Anzilotti, C., Fischer, R., Deobagkar-Lele, M., Sanchiz-Calvo, M., Fueyo-Marcos, E., et al. (2018). 53BP1 cooperation with the REV7-shieldin complex underpins DNA structure-specific NHEJ. Nature *560*, 122–127. https://doi.org/10.1038/s41586-018-0362-1.
14. Noordermeer, S.M., Adam, S., Setiaputra, D., Barazas, M., Pettitt, S.J., Ling, A.K., Olivieri, M., Álvarez-Quilón, A., Moatti, N., Zimmermann, M., et al. (2018). The shieldin complex mediates 53BP1-dependent DNA repair. Nature *560*, 117–121. https://doi.org/10.1038/s41586-018-0340-7.
15. Alt, F.W., Zhang, Y., Meng, F.L., Guo, C., and Schwer, B. (2013). Mechanisms of programmed DNA lesions and genomic instability in the immune system. Cell *152*, 417–429. https://doi.org/10.1016/j.cell.2013.01.007.
16. Stavnezer, J., and Schrader, C.E. (2014). IgH chain class switch recombination: mechanism and regulation. J. Immunol. *193*, 5370–5378. https://doi.org/10.4049/jimmunol.1401849.

17. Yan, C.T., Boboila, C., Souza, E.K., Franco, S., Hickernell, T.R., Murphy, M., Gumaste, S., Geyer, M., Zarrin, A.A., Manis, J.P., et al. (2007). IgH class switching and translocations use a robust non-classical end-joining pathway. Nature *449*, 478–482. https://doi.org/10.1038/nature06020.

18. Lu, W.T., Hawley, B.R., Skalka, G.L., Baldock, R.A., Smith, E.M., Bader, A.S., Malewicz, M., Watts, F.Z., Wilczynska, A., and Bushell, M. (2018). Drosha drives the formation of DNA:RNA hybrids around DNA break sites to facilitate DNA repair. Nat. Commun. *9*, 532. https://doi.org/10.1038/s41467-018-02893-x.

19. Ohle, C., Tesorero, R., Schermann, G., Dobrev, N., Sinning, I., and Fischer, T. (2016). Transient RNA-DNA hybrids are required for efficient double-strand break repair. Cell *167*, 1001–1013.e7. https://doi.org/10.1016/j.cell.2016.10.001.

20. Liu, S., Hua, Y., Wang, J., Li, L., Yuan, J., Zhang, B., Wang, Z., Ji, J., and Kong, D. (2021). RNA polymerase III is required for the repair of DNA double-strand breaks by homologous recombination. Cell *184*, 1314–1329.e10. https://doi.org/10.1016/j.cell.2021.01.048.

21. Keskin, H., Shen, Y., Huang, F., Patel, M., Yang, T., Ashley, K., Mazin, A.V., and Storici, F. (2014). Transcript-RNA-templated DNA recombination and repair. Nature *515*, 436–439. https://doi.org/10.1038/nature13682.

22. Michelini, F., Pitchiaya, S., Vitelli, V., Sharma, S., Gioia, U., Pessina, F., Cabrini, M., Wang, Y., Capozzo, I., Iannelli, F., et al. (2017). Damage-induced lncRNAs control the DNA damage response through interaction with DDRNAs at individual double-strand breaks. Nat. Cell Biol. *19*, 1400–1411. https://doi.org/10.1038/ncb3643.

23. Zhang, Z.Z., Pannunzio, N.R., Hsieh, C.L., Yu, K., and Lieber, M.R. (2014). The role of G-density in switch region repeats for immunoglobulin class switch recombination. Nucleic Acids Res. *42*, 13186–13193. https://doi.org/10.1093/nar/gku1100.

24. Yu, K., Chedin, F., Hsieh, C.L., Wilson, T.E., and Lieber, M.R. (2003). R-loops at immunoglobulin class switch regions in the chromosomes of stimulated B cells. Nat. Immunol. *4*, 442–451. https://doi.org/10.1038/ni919.

25. Qiao, Q., Wang, L., Meng, F.L., Hwang, J.K., Alt, F.W., and Wu, H. (2017). AID recognizes structured DNA for class switch recombination. Mol. Cell *67*, 361–373.e4. https://doi.org/10.1016/j.molcel.2017.06.034.

26. Crossley, M.P., Bocek, M., and Cimprich, K.A. (2019). R-loops as cellular regulators and genomic threats. Mol. Cell *73*, 398–411. https://doi.org/10.1016/j.molcel.2019.01.024.

27. Hamperl, S., and Cimprich, K.A. (2014). The contribution of co-transcriptional RNA: DNA hybrid structures to DNA damage and genome instability. DNA Repair *19*, 84–94. https://doi.org/10.1016/j.dnarep.2014.03.023.

28. Aguilera, A., and Gómez-González, B. (2017). DNA-RNA hybrids: the risks of DNA breakage during transcription. Nat. Struct. Mol. Biol. *24*, 439–443. https://doi.org/10.1038/nsmb.3395.

29. Yasuhara, T., Kato, R., Hagiwara, Y., Shiotani, B., Yamauchi, M., Nakada, S., Shibata, A., and Miyagawa, K. (2018). Human Rad52 promotes XPG-mediated R-loop processing to initiate transcription-associated homologous recombination repair. Cell *175*, 558–570.e11. https://doi.org/10.1016/j.cell.2018.08.056.

30. Laffleur, B., Lim, J., Zhang, W., Chen, Y., Pefanis, E., Bizarro, J., Batista, C.R., Wu, L., Economides, A.N., Wang, J., and Basu, U. (2021). Noncoding RNA processing by DIS3 regulates chromosomal architecture and somatic hypermutation in B cells. Nat. Genet. *53*, 230–242. https://doi.org/10.1038/s41588-020-00772-0.

31. Nair, L., Zhang, W., Laffleur, B., Jha, M.K., Lim, J., Lee, H., Wu, L., Alvarez, N.S., Liu, Z.P., Munteanu, E.L., et al. (2021). Mechanism of noncoding RNA-associated N(6)-methyladenosine recognition by an RNA processing complex during IgH DNA recombination. Mol. Cell *81*, 3949–3964.e7. https://doi.org/10.1016/j.molcel.2021.07.037.

32. Perlot, T., Li, G., and Alt, F.W. (2008). Antisense transcripts from immunoglobulin heavy-chain locus V(D)J and switch regions. Proc. Natl. Acad. Sci. USA *105*, 3843–3848. https://doi.org/10.1073/pnas.0712291105.

33. Wiedemann, E.M., Peycheva, M., and Pavri, R. (2016). DNA replication origins in immunoglobulin switch regions regulate class switch recombination in an R-loop-dependent manner. Cell Rep. *17*, 2927–2942. https://doi.org/10.1016/j.celrep.2016.11.041.

34. Ribeiro de Almeida, C., Dhir, S., Dhir, A., Moghaddam, A.E., Sattentau, Q., Meinhart, A., and Proudfoot, N.J. (2018). RNA helicase DDX1 converts RNA G-quadruplex structures into R-loops to promote IgH class switch recombination. Mol. Cell *70*, 650–662.e8. https://doi.org/10.1016/j.molcel.2018.04.001.

35. Izumi, H., and Funa, K. (2019). Telomere function and the G-quadruplex formation are regulated by hnRNP U. Cells *8*, 390. https://doi.org/10.3390/cells8050390.

36. Kiledjian, M., and Dreyfuss, G. (1992). Primary structure and binding activity of the hnRNP U protein: binding RNA through RGG box. EMBO J. *11*, 2655–2664.

37. Hu, W., Begum, N.A., Mondal, S., Stanlie, A., and Honjo, T. (2015). Identification of DNA cleavage- and recombination-specific hnRNP cofactors for activation-induced cytidine deaminase. Proc. Natl. Acad. Sci. USA *112*, 5791–5796. https://doi.org/10.1073/pnas.1506167112.

38. Mondal, S., Begum, N.A., Hu, W., and Honjo, T. (2016). Functional requirements of AID's higher order structures and their interaction with RNA-binding proteins. Proc. Natl. Acad. Sci. USA *113*, E1545–E1554. https://doi.org/10.1073/pnas.1601678113.

39. Nakamura, M., Kondo, S., Sugai, M., Nazarea, M., Imamura, S., and Honjo, T. (1996). High frequency class switching of an IgM+ B lymphoma clone CH12F3 to IgA+ cells. Int. Immunol. *8*, 193–201. https://doi.org/10.1093/intimm/8.2.193.

40. Boboila, C., Alt, F.W., and Schwer, B. (2012). Classical and alternative end-joining pathways for repair of lymphocyte-specific and general DNA double-strand breaks. Adv. Immunol. *116*, 1–49. https://doi.org/10.1016/B978-0-12-394300-2.00001-6.

41. Chang, H.H.Y., Pannunzio, N.R., Adachi, N., and Lieber, M.R. (2017). Non-homologous DNA end joining and alternative pathways to double-strand break repair. Nat. Rev. Mol. Cell Biol. *18*, 495–506. https://doi.org/10.1038/nrm.2017.48.

42. Gupta, R., Somyajit, K., Narita, T., Maskey, E., Stanlie, A., Kremer, M., Typas, D., Lammers, M., Mailand, N., Nussenzweig, A., et al. (2018). DNA repair network analysis reveals shieldin as a key regulator of NHEJ and PARP inhibitor sensitivity. Cell *173*, 972–988.e23. https://doi.org/10.1016/j.cell.2018.03.050.

43. Li, C., Irrazabal, T., So, C.C., Berru, M., Du, L., Lam, E., Ling, A.K., Gommerman, J.L., Pan-Hammarström, Q., and Martin, A. (2018). The H2B deubiquitinase Usp22 promotes antibody class switch recombination by facilitating non-homologous end joining. Nat. Commun. *9*, 1006. https://doi.org/10.1038/s41467-018-03455-x.

44. Reina-San-Martin, B., Chen, J., Nussenzweig, A., and Nussenzweig, M.C. (2007). Enhanced intra-switch region recombination during immunoglobulin class switch recombination in 53BP1-/- B cells. Eur. J. Immunol. *37*, 235–239. https://doi.org/10.1002/eji.200636789.

45. Ramiro, A.R., Jankovic, M., Callen, E., Difilippantonio, S., Chen, H.T., McBride, K.M., Eisenreich, T.R., Chen, J., Dickins, R.A., Lowe, S.W., et al. (2006). Role of genomic instability and p53 in AID-induced c-myc-Igh translocations. Nature *440*, 105–109. https://doi.org/10.1038/nature04495.

46. Bunting, S.F., Callén, E., Wong, N., Chen, H.T., Polato, F., Gunn, A., Bothmer, A., Feldhahn, N., Fernandez-Capetillo, O., Cao, L., et al. (2010). 53BP1 inhibits homologous recombination in Brca1-deficient cells by blocking resection of DNA breaks. Cell *141*, 243–254. https://doi.org/10.1016/j.cell.2010.03.012.

47. Montecucco, A., Zanetta, F., and Biamonti, G. (2015). Molecular mechanisms of etoposide. EXCLI J. *14*, 95–108. https://doi.org/10.17179/excli2015-561.

48. Quennet, V., Beucher, A., Barton, O., Takeda, S., and Löbrich, M. (2011). CtIP and MRN promote non-homologous end-joining of etoposide-induced DNA double-strand breaks in G1. Nucleic Acids Res. *39*, 2144–2152. https://doi.org/10.1093/nar/gkq1175.

49. Kuntz, K., and O'Connell, M.J. (2013). Initiation of DNA damage responses through XPG-related nucleases. EMBO J. *32*, 290–302. https://doi.org/10.1038/emboj.2012.322.

50. Zhao, F., Kim, W., Gao, H., Liu, C., Zhang, Y., Chen, Y., Deng, M., Zhou, Q., Huang, J., Hu, Q., et al. (2021). ASTE1 promotes shieldin-complex-mediated DNA repair by attenuating end resection. Nat. Cell Biol. *23*, 894–904. https://doi.org/10.1038/s41556-021-00723-9.

51. Britton, S., Dernoncourt, E., Delteil, C., Froment, C., Schiltz, O., Salles, B., Frit, P., and Calsou, P. (2014). DNA damage triggers SAF-A and RNA biogenesis factors exclusion from chromatin coupled to R-loops removal. Nucleic Acids Res. *42*, 9047–9062. https://doi.org/10.1093/nar/gku601.

52. Wu, X., Wilson, T.E., and Lieber, M.R. (1999). A role for FEN-1 in nonhomologous DNA end joining: the order of strand annealing and nucleolytic processing events. Proc. Natl. Acad. Sci. USA *96*, 1303–1308. https://doi.org/10.1073/pnas.96.4.1303.

53. Gibbons, H.R., and Aune, T.M. (2020). Immunoprecipitation of DNA:RNA hybrids using the S9.6 antibody. Methods Mol. Biol. *2161*, 195–207. https://doi.org/10.1007/978-1-0716-0680-3_14.

54. Robbiani, D.F., and Nussenzweig, M.C. (2013). Chromosome translocation, B cell lymphoma, and activation-induced cytidine deaminase. Annu. Rev. Pathol. *8*, 79–103. https://doi.org/10.1146/annurev-pathol-020712-164004.

55. Chen, L., Chen, J.Y., Zhang, X., Gu, Y., Xiao, R., Shao, C., Tang, P., Qian, H., Luo, D., Li, H., et al. (2017). R-ChIP using inactive RNase H reveals dynamic coupling of R-loops with transcriptional pausing at gene promoters. Mol. Cell *68*, 745–757.e5. https://doi.org/10.1016/j.molcel.2017.10.008.

56. Nowotny, M., Cerritelli, S.M., Ghirlando, R., Gaidamakov, S.A., Crouch, R.J., and Yang, W. (2008). Specific recognition of RNA/DNA hybrid and enhancement of human RNase H1 activity by HBD. EMBO J. *27*, 1172–1181. https://doi.org/10.1038/emboj.2008.44.

57. Cristini, A., Groh, M., Kristiansen, M.S., and Gromak, N. (2018). RNA/DNA hybrid interactome identifies DXH9 as a molecular player in transcriptional termination and R-loop-associated DNA damage. Cell Rep. *23*, 1891–1905. https://doi.org/10.1016/j.celrep.2018.04.025.

58. Maréchal, A., and Zou, L. (2015). RPA-coated single-stranded DNA as a platform for post-translational modifications in the DNA damage response. Cell Res. *25*, 9–23. https://doi.org/10.1038/cr.2014.147.

59. Nguyen, H.D., Yadav, T., Giri, S., Saez, B., Graubert, T.A., and Zou, L. (2017). Functions of replication protein A as a sensor of R loops and a regulator of RNaseH1. Mol. Cell *65*, 832–847.e4. https://doi.org/10.1016/j.molcel.2017.01.029.

60. Zheng, S., Vuong, B.Q., Vaidyanathan, B., Lin, J.Y., Huang, F.T., and Chaudhuri, J. (2015). Non-coding RNA generated following lariat debranching mediates targeting of AID to DNA. Cell *161*, 762–773. https://doi.org/10.1016/j.cell.2015.03.020.

61. Vuong, B.Q., Herrick-Reynolds, K., Vaidyanathan, B., Pucella, J.N., Ucher, A.J., Donghia, N.M., Gu, X., Nicolas, L., Nowak, U., Rahman, N., et al. (2013). A DNA break- and phosphorylation-dependent positive feedback loop promotes immunoglobulin class-switch recombination. Nat. Immunol. *14*, 1183–1189. https://doi.org/10.1038/ni.2732.

62. Pucella, J.N., and Chaudhuri, J. (2017). AID invited to the G4 summit. Mol. Cell *67*, 355–357. https://doi.org/10.1016/j.molcel.2017.07.020.

63. Zhang, Y., He, Q., Hu, Z., Feng, Y., Fan, L., Tang, Z., Yuan, J., Shan, W., Li, C., Hu, X., et al. (2016). Long noncoding RNA LINP1 regulates repair of DNA double-strand breaks in triple-negative breast cancer. Nat. Struct. Mol. Biol. *23*, 522–530. https://doi.org/10.1038/nsmb.3211.

64. Wang, X., Liu, H., Shi, L., Yu, X., Gu, Y., and Sun, X. (2018). LINP1 facilitates DNA damage repair through non-homologous end joining (NHEJ) pathway and subsequently decreases the sensitivity of cervical cancer cells to ionizing radiation. Cell Cycle *17*, 439–447. https://doi.org/10.1080/15384101.2018.1442625.

65. Altmeyer, M., Neelsen, K.J., Teloni, F., Pozdnyakova, I., Pellegrino, S., Grøfte, M., Rask, M.B.D., Streicher, W., Jungmichel, S., Nielsen, M.L., and Lukas, J. (2015). Liquid demixing of intrinsically disordered proteins is seeded by poly(ADP-ribose). Nat. Commun. *6*, 8088. https://doi.org/10.1038/ncomms9088.

66. Pessina, F., Giavazzi, F., Yin, Y., Gioia, U., Vitelli, V., Galbiati, A., Barozzi, S., Garre, M., Oldani, A., Flaus, A., et al. (2019). Functional transcription promoters at DNA double-strand breaks mediate RNA-driven phase separation of damage-response factors. Nat. Cell Biol. *21*, 1286–1299. https://doi.org/10.1038/s41556-019-0392-4.

67. Kilic, S., Lezaja, A., Gatti, M., Bianco, E., Michelena, J., Imhof, R., and Altmeyer, M. (2019). Phase separation of 53BP1 determines liquid-like behavior of DNA repair compartments. EMBO J. *38*, e101379. https://doi.org/10.15252/embj.2018101379.

68. Fijen, C., and Rothenberg, E. (2021). The evolving complexity of DNA damage foci: RNA, condensates and chromatin in DNA double-strand break repair. DNA Repair *105*, 103170. https://doi.org/10.1016/j.dnarep.2021.103170.

69. Wang, Y.L., Zhao, W.W., Bai, S.M., Feng, L.L., Bie, S.Y., Gong, L., Wang, F., Wei, M.B., Feng, W.X., Pang, X.L., et al. (2022). MRNIP condensates promote DNA double-strand break sensing and end resection. Nat. Commun. *13*, 2638. https://doi.org/10.1038/s41467-022-30303-w.

70. Kato, M., Han, T.W., Xie, S., Shi, K., Du, X., Wu, L.C., Mirzaei, H., Goldsmith, E.J., Longgood, J., Pei, J., et al. (2012). Cell-free formation of RNA granules: low complexity sequence domains form dynamic fibers within hydrogels. Cell *149*, 753–767. https://doi.org/10.1016/j.cell.2012.04.017.

71. Xie, X., Gan, T., Rao, B., Zhang, W., Panchakshari, R.A., Yang, D., Ji, X., Cao, Y., Alt, F.W., Meng, F.L., and Hu, J. (2022). C-terminal deletion-induced condensation sequesters AID from IgH targets in immunodeficiency. EMBO J. *41*, e109324. https://doi.org/10.15252/embj.2021109324.

72. Kroschwald, S., Maharana, S., and Simon, A. (2017). Hexanediol: a chemical probe to investigate the material properties of membrane-less compartments. Matters *3*. e201702000010.

73. Strom, A.R., Emelyanov, A.V., Mir, M., Fyodorov, D.V., Darzacq, X., and Karpen, G.H. (2017). Phase separation drives heterochromatin domain formation. Nature *547*, 241–245. https://doi.org/10.1038/nature22989.

74. Jain, A., and Vale, R.D. (2017). RNA phase transitions in repeat expansion disorders. Nature *546*, 243–247. https://doi.org/10.1038/nature22386.

75. Lee-Theilen, M., Matthews, A.J., Kelly, D., Zheng, S., and Chaudhuri, J. (2011). CtIP promotes microhomology-mediated alternative end joining during class-switch recombination. Nat. Struct. Mol. Biol. *18*, 75–79. https://doi.org/10.1038/nsmb.1942.

76. Panchakshari, R.A., Zhang, X., Kumar, V., Du, Z., Wei, P.C., Kao, J., Dong, J., and Alt, F.W. (2018). DNA double-strand break response factors influence end-joining features of IgH class switch and general translocation junctions. Proc. Natl. Acad. Sci. USA *115*, 762–767. https://doi.org/10.1073/pnas.1719988115.

77. Ghezraoui, H., Piganeau, M., Renouf, B., Renaud, J.B., Sallmyr, A., Ruis, B., Oh, S., Tomkinson, A.E., Hendrickson, E.A., Giovannangeli, C., et al. (2014). Chromosomal translocations in human cells are generated by canonical nonhomologous end-joining. Mol. Cell *55*, 829–842. https://doi.org/10.1016/j.molcel.2014.08.002.

78. Husain, A., Xu, J., Fujii, H., Nakata, M., Kobayashi, M., Wang, J.Y., Rehwinkel, J., Honjo, T., and Begum, N.A. (2020). SAMHD1-mediated

dNTP degradation is required for efficient DNA repair during antibody class switch recombination. EMBO J. *39*, e102931. https://doi.org/10.15252/embj.2019102931.

79. Jaafar, L., Li, Z., Li, S., and Dynan, W.S. (2017). SFPQ*NONO and XLF function separately and together to promote DNA double-strand break repair via canonical nonhomologous end joining. Nucleic Acids Res. *45*, 1848–1859. https://doi.org/10.1093/nar/gkw1209.

80. Petti, E., Buemi, V., Zappone, A., Schillaci, O., Broccia, P.V., Dinami, R., Matteoni, S., Benetti, R., and Schoeftner, S. (2019). SFPQ and NONO suppress RNA:DNA-hybrid-related telomere instability. Nat. Commun. *10*, 1001. https://doi.org/10.1038/s41467-019-08863-1.

81. Pryde, F., Khalili, S., Robertson, K., Selfridge, J., Ritchie, A.M., Melton, D.W., Jullien, D., and Adachi, Y. (2005). 53BP1 exchanges slowly at the sites of DNA damage and appears to require RNA for its association with chromatin. J. Cell Sci. *118*, 2043–2055. https://doi.org/10.1242/jcs.02336.

82. Dynan, W.S., and Yoo, S. (1998). Interaction of Ku protein and DNA-dependent protein kinase catalytic subunit with nucleic acids. Nucleic Acids Res. *26*, 1551–1559. https://doi.org/10.1093/nar/26.7.1551.

83. Thapar, R., Wang, J.L., Hammel, M., Ye, R., Liang, K., Sun, C., Hnizda, A., Liang, S., Maw, S.S., Lee, L., et al. (2020). Mechanism of efficient double-strand break repair by a long non-coding RNA. Nucleic Acids Res. *48*, 10953–10972. https://doi.org/10.1093/nar/gkaa784.

84. Chakraborty, A., Tapryal, N., Venkova, T., Horikoshi, N., Pandita, R.K., Sarker, A.H., Sarkar, P.S., Pandita, T.K., and Hazra, T.K. (2016). Classical non-homologous end-joining pathway utilizes nascent RNA for error-free double-strand break repair of transcribed genes. Nat. Commun. *7*, 13049. https://doi.org/10.1038/ncomms13049.

85. Jimeno, S., Prados-Carvajal, R., and Huertas, P. (2019). The role of RNA and RNA-related proteins in the regulation of DNA double strand break repair pathway choice. DNA Repair *81*, 102662. https://doi.org/10.1016/j.dnarep.2019.102662.

86. Fan, H., Lv, P., Huo, X., Wu, J., Wang, Q., Cheng, L., Liu, Y., Tang, Q.Q., Zhang, L., Zhang, F., et al. (2018). The nuclear matrix protein HNRNPU maintains 3D genome architecture globally in mouse hepatocytes. Genome Res. *28*, 192–202. https://doi.org/10.1101/gr.224576.117.

87. Nozawa, R.S., Boteva, L., Soares, D.C., Naughton, C., Dun, A.R., Buckle, A., Ramsahoye, B., Bruton, P.C., Saleeb, R.S., Arnedo, M., et al. (2017). SAF-A regulates interphase chromosome structure through oligomerization with chromatin-associated RNAs. Cell *169*, 1214–1227.e18. https://doi.org/10.1016/j.cell.2017.05.029.

88. Hacisuleyman, E., Goff, L.A., Trapnell, C., Williams, A., Henao-Mejia, J., Sun, L., McClanahan, P., Hendrickson, D.G., Sauvageau, M., Kelley, D.R., et al. (2014). Topological organization of multichromosomal regions by the long intergenic noncoding RNA Firre. Nat. Struct. Mol. Biol. *21*, 198–206. https://doi.org/10.1038/nsmb.2764.

89. Creamer, K.M., Kolpa, H.J., and Lawrence, J.B. (2021). Nascent RNA scaffolds contribute to chromosome territory architecture and counter chromatin compaction. Mol. Cell *81*, 3509–3525.e5. https://doi.org/10.1016/j.molcel.2021.07.004.

90. Sakaguchi, T., Hasegawa, Y., Brockdorff, N., Tsutsui, K., Tsutsui, K.M., Sado, T., and Nakagawa, S. (2016). Control of chromosomal localization of xist by hnRNP U family molecules. Dev. Cell *39*, 11–12. https://doi.org/10.1016/j.devcel.2016.09.022.

91. Nozawa, R.S., and Gilbert, N. (2019). RNA: nuclear glue for folding the genome. Trends Cell Biol. *29*, 201–211. https://doi.org/10.1016/j.tcb.2018.12.003.

92. Patel, A., Lee, H.O., Jawerth, L., Maharana, S., Jahnel, M., Hein, M.Y., Stoynov, S., Mahamid, J., Saha, S., Franzmann, T.M., et al. (2015). A liquid-to-solid phase transition of the ALS protein FUS accelerated by disease mutation. Cell *162*, 1066–1077. https://doi.org/10.1016/j.cell.2015.07.047.

93. Jang, Y., Elsayed, Z., Eki, R., He, S., Du, K.P., Abbas, T., and Kai, M. (2020). Intrinsically disordered protein RBM14 plays a role in generation of RNA:DNA hybrids at double-strand break sites. Proc. Natl. Acad. Sci. USA *117*, 5329–5338. https://doi.org/10.1073/pnas.1913280117.

94. Zhang, Y., Yang, M., Duncan, S., Yang, X., Abdelhamid, M.A.S., Huang, L., Zhang, H., Benfey, P.N., Waller, Z.A.E., and Ding, Y. (2019). G-quadruplex structures trigger RNA phase separation. Nucleic Acids Res. *47*, 11746–11754. https://doi.org/10.1093/nar/gkz978.

95. de Lange, T. (2018). Shelterin-mediated telomere protection. Annu. Rev. Genet. *52*, 223–247. https://doi.org/10.1146/annurev-genet-032918-021921.

96. Masai, H., Fukatsu, R., Kakusho, N., Kanoh, Y., Moriyama, K., Ma, Y., Iida, K., and Nagasawa, K. (2019). Rif1 promotes association of G-quadruplex (G4) by its specific G4 binding and oligomerization activities. Sci. Rep. *9*, 8618. https://doi.org/10.1038/s41598-019-44736-9.

97. Moriyama, K., Yoshizawa-Sugata, N., and Masai, H. (2018). Oligomer formation and G-quadruplex binding by purified murine Rif1 protein, a key organizer of higher-order chromatin architecture. J. Biol. Chem. *293*, 3607–3624. https://doi.org/10.1074/jbc.RA117.000446.

98. De Magis, A., Götz, S., Hajikazemi, M., Fekete-Szücs, E., Caterino, M., Juranek, S., and Paeschke, K. (2020). Zuo1 supports G4 structure formation and directs repair toward nucleotide excision repair. Nat. Commun. *11*, 3907. https://doi.org/10.1038/s41467-020-17701-8.

99. Boán, F., and Gómez-Márquez, J. (2010). In vitro recombination mediated by G-quadruplexes. Chembiochem *11*, 331–334. https://doi.org/10.1002/cbic.200900612.

100. Muniyappa, K., Anuradha, S., and Byers, B. (2000). Yeast meiosis-specific protein Hop1 binds to G4 DNA and promotes its formation. Mol. Cell Biol. *20*, 1361–1369. https://doi.org/10.1128/MCB.20.4.1361-1369.2000.

101. Nishida, K., Kuwano, Y., Nishikawa, T., Masuda, K., and Rokutan, K. (2017). RNA binding proteins and genome integrity. Int. J. Mol. Sci. *18*, 1341. https://doi.org/10.3390/ijms18071341.

102. Stanlie, A., Aida, M., Muramatsu, M., Honjo, T., and Begum, N.A. (2010). Histone3 lysine4 trimethylation regulated by the facilitates chromatin transcription complex is critical for DNA cleavage in class switch recombination. Proc. Natl. Acad. Sci. USA *107*, 22190–22195. https://doi.org/10.1073/pnas.1016923108.

103. Nagaoka, H., Muramatsu, M., Yamamura, N., Kinoshita, K., and Honjo, T. (2002). Activation-induced deaminase (AID)-directed hypermutation in the immunoglobulin Smu region: implication of AID involvement in a common step of class switch recombination and somatic hypermutation. J. Exp. Med. *195*, 529–534. https://doi.org/10.1084/jem.20012144.

104. Shinkura, R., Ito, S., Begum, N.A., Nagaoka, H., Muramatsu, M., Kinoshita, K., Sakakibara, Y., Hijikata, H., and Honjo, T. (2004). Separate domains of AID are required for somatic hypermutation and class-switch recombination. Nat. Immunol. *5*, 707–712. https://doi.org/10.1038/ni1086.

105. Ramiro, A.R., Jankovic, M., Eisenreich, T., Difilippantonio, S., Chen-Kiang, S., Muramatsu, M., Honjo, T., Nussenzweig, A., and Nussenzweig, M.C. (2004). AID is required for c-myc/IgH chromosome translocations in vivo. Cell *118*, 431–438. https://doi.org/10.1016/j.cell.2004.08.006.

106. Boboila, C., Oksenych, V., Gostissa, M., Wang, J.H., Zha, S., Zhang, Y., Chai, H., Lee, C.S., Jankovic, M., Saez, L.M.A., et al. (2012). Robust chromosomal DNA repair via alternative end-joining in the absence of X-ray repair cross-complementing protein 1 (XRCC1). Proc. Natl. Acad. Sci. USA *109*, 2473–2478. https://doi.org/10.1073/pnas.1121470109.

107. Rush, J.S., Fugmann, S.D., and Schatz, D.G. (2004). Staggered AID-dependent DNA double strand breaks are the predominant DNA lesions targeted to S mu in Ig class switch recombination. Int. Immunol. *16*, 549–557. https://doi.org/10.1093/intimm/dxh057.

108. Schrader, C.E., Linehan, E.K., Mochegova, S.N., Woodland, R.T., and Stavnezer, J. (2005). Inducible DNA breaks in Ig S regions are dependent

on AID and UNG. J. Exp. Med. *202*, 561–568. https://doi.org/10.1084/jem.20050872.

109. Guikema, J.E.J., Linehan, E.K., Tsuchimoto, D., Nakabeppu, Y., Strauss, P.R., Stavnezer, J., and Schrader, C.E. (2007). APE1- and APE2-dependent DNA breaks in immunoglobulin class switch recombination. J. Exp. Med. *204*, 3017–3026. https://doi.org/10.1084/jem.20071289.

110. Methot, S.P., Litzler, L.C., Subramani, P.G., Eranki, A.K., Fifield, H., Patenaude, A.M., Gilmore, J.C., Santiago, G.E., Bagci, H., Côté, J.F., et al. (2018). A licensing step links AID to transcription elongation for mutagenesis in B cells. Nat. Commun. *9*, 1248. https://doi.org/10.1038/s41467-018-03387-6.

111. Zhang, Z.Z., Pannunzio, N.R., Han, L., Hsieh, C.L., Yu, K., and Lieber, M.R. (2014). The strength of an Ig switch region is determined by its ability to drive R loop formation and its number of WGCW sites. Cell Rep. *8*, 557–569. https://doi.org/10.1016/j.celrep.2014.06.021.

112. Zhang, Z.Z., Pannunzio, N.R., Hsieh, C.L., Yu, K., and Lieber, M.R. (2015). Complexities due to single-stranded RNA during antibody detection of genomic rna:dna hybrids. BMC Res. Notes *8*, 127. https://doi.org/10.1186/s13104-015-1092-1.

113. Britton, S., Coates, J., and Jackson, S.P. (2013). A new method for high-resolution imaging of Ku foci to decipher mechanisms of DNA double-strand break repair. J. Cell Biol. *202*, 579–595. https://doi.org/10.1083/jcb.201303073.

114. Lim, K.K., and Chen, E.S. (2018). Systematic quantification of GFP-tagged protein foci in Schizosaccharomyces pombe nuclei. Bio. Protoc. *8*, e3117. https://doi.org/10.21769/BioProtoc.3117.

115. Nair, S.J., Yang, L., Meluzzi, D., Oh, S., Yang, F., Friedman, M.J., Wang, S., Suter, T., Alshareedah, I., Gamliel, A., et al. (2019). Phase separation of ligand-activated enhancers licenses cooperative chromosomal enhancer assembly. Nat. Struct. Mol. Biol. *26*, 193–203. https://doi.org/10.1038/s41594-019-0190-5.

STAR★METHODS

KEY RESOURCES TABLE

REAGENT or RESOURCE	SOURCE	IDENTIFIER
Antibodies		
Anti-IgA-PE	Southern Biotech	Cat# 1040-09; RRID: AB_2794375
Anti-IgM-FITC	eBioscience	Cat# 1-5890-85; RRID: AB_465291
Rabbit IgG	Millipore	Cat# PP64B; RRID: AB_1977567
Anti- IgG1	BD Pharmingen	Cat# 553441; RRID: AB_394861
Anti-KU80	Santa Cruz	Cat# sc-1485; RRID: AB_2288756
Anti-KU80	Santa Cruz	Cat# sc-5280; RRID: AB_672929
Anti-AID	Cell Signaling	Cat# 4949s; RRID: AB_2258037
Anti-HNRNPU	Santa Cruz	Cat# sc-32315; RRID: AB_627741
Anti-ASTE1	NovusBIO	Cat# NBP1-81661; RRID: AB_11031613
Anti-FLAG M2	Sigma	Cat# F-3165; RRID: AB_259529
Anti-FLAG Agarose	Sigma	Cat# A2220; RRID: AB_10063035
Halo-Trap Agarose	ChromoTek	Cat# ota-10; RRID: AB_2827595
Anti-GFP Agarose	MBL	Cat# D153-8; RRID: AB_591815
Anti-RPA32	Abcam	Cat# ab10359; RRID: AB_297095
Anti-Phospho RPA32	Bethyl	Cat# A300-245A; RRID: AB_210547
Anti-DHX36	Proteintech	Cat# 13159-1-AP; RRID: AB_2092157
Anti-H3S10P	Active Motif	Cat# 39253; RRID: AB_2793206
Anti-mouse-HRP	Rockland	Cat# 18-8817-33; RRID: AB_2610851
Anti-rabbit-HRP	Rockland	Cat# 18-8816-33; RRID: AB_2610848
Anti-TUBULIN	Calbiochem	Cat# CP06; RRID: AB_2617116
Anti-SFPQ	Abcam	Cat# ab38148; RRID: AB_945424
Anti-NONO	Abcam	Cat# ab70335; RRID: AB_1269576
Anti-53BP1	NovusBIO	Cat# NB100-304; RRID: AB_10003037
Anti-53BP1	Santa Cruz	Cat# sc-22760; RRID: AB_2256326
Anti-DNA-PKcs	Santa Cruz	Cat# sc-5282; RRID: AB_2172848
Anti-GAPDH	Millipore	Cat# MAB374; RRID: AB_2107445
Anti-CTCF	Millipore	Cat# 07-729; RRID: AB_441965
Anti-FEN1	Bethyl	Cat# A300-255A; RRID: AB_185550
Anti-TOP1	BD Bioscience	Cat# 556597; RRID: AB_396474
Anti-BRCA1	Proteintech	Cat# 22362-1-AP; RRID: AB_2879090
Anti-γH2AX	Millipore	Cat# 05-636; RRID: AB_309864
Anti-DHX9	Proteintech	Cat# 17721-1-AP; RRID: AB_2092506
Anti-DDX1	Proteintech	Cat# 11357-1-AP; RRID: AB_2092222
Anti-DDX5	Bethyl	Cat# A300-523A; RRID: AB_451048
Anti-V5 Agarose	Abcam	Cat# ab1229; RRID: AB_308681
Anti-rabbit Alexa 488	Abcam	Cat# ab150077; RRID: AB_2630356
Anti-mouse Alexa 647	Abcam	Cat# ab150115; RRID: AB_2687948
Anti-V5	Abcam	Cat# ab9116; RRID: AB_307024
Chemicals, peptides, and recombinant proteins		
mCD40L supernatant	Dr. Tasuko Honjo's Lab	N/A
TGF-β	R&D Systems	Cat# 240-B-010
IL-4	WAKO	Cat# 090-06621
QuickChange Site-Directed Mutagenesis Kit	New England Biolabs	Cat# E0552S
Expand Long Template PCR System	Roche	Cat# 11 681,842 001

(*Continued on next page*)

Continued

REAGENT or RESOURCE	SOURCE	IDENTIFIER
PrimeSTAR HS DNA Polymerase	Takara	Cat# R010A
LaTaq DNA Polymerase	Takara	Cat# R001
Pyrobest DNA Polymerase	Takara	Cat# R005B
SuperScript IV Reverse Transcriptase	Thermo Fisher Scientific	Cat# 18090050
KOD FX *Neo* DNA Polymerase	TOYOBO	Cat# KFX-201
PowerUp SYBR Green Master Mix	Applied Biosystems	Cat# A25742
Expand Long Template PCR System	Roche	Cat# 11681842001
T4 DNA polymerase	Takara	Cat# 2040A
BD IMag Anti-PE Magnetic Particles DM	BD Biosciences	Cat# 557899
Dynabeads Protein G	Thermo Fisher Scientific	Cat# 10003D
Dynabeads M-280 Streptavidin	Thermo Fisher Scientific	Cat# 11205D
Streptavidin (HRP)	Abcam	Cat# ab7403
Lipofectamine 2000	Thermo Fisher Scientific	Cat# 11668027
SF Cell line 96-well Nucleofector Kit	Lonza	Cat# V4SC-2096
Subcellular Protein Fractionation Kit	Thermo Fisher Scientific	Cat# 78840
Mouse B lymphocyte enrichment kit	BD Biosciences	Cat# 557792
NE-PER Nuclear and Cytoplasmic Extraction	Thermo Fisher Scientific	Cat# 78833
ChIP DNA Clean & Concentrator	Zymo Research	Cat# D5201
RNase H	Takara	Cat# 2150A
RNase A	Nippon Gene	Cat# 312-01931
EDTA free protease inhibitors	Roche	Cat# 5056489001
RNase Inhibitor	Invitrogen	Cat# 10777019
Ammonium Acetate (NH4OAc)	Thermo Fisher Scientific	Cat# AM9070G
1,6-Hexanediol (1,6-HD)	Sigma	Cat# 88571
Sorbitol	Sigma	Cat# S3889
Biotinylated isoxazole	Sigma	Cat# 900572
ChIP-IT Express Kit	Active Motif	Cat# 53008
Experimental models: Cell lines		
HEK 293T	ATCC	CRL-3216
Murine: CH12 (CH12F3-2A): WT	Nakamura et al.[39]	N/A
Murine: CH12.Bcl2 (Expressing hBcl2)	Stanlie et al.[102]	N/A
Murine: CH12_*53bp1*$^{-/-}$ (*53bp1* ^{KO})	Gupta et al.[42]	N/A
Murine: CH12_*Shld1*$^{-/-}$ (*Shld1* ^{KO})	Gupta et al.[42]	N/A
Murine: CH12_*Shld3*$^{-/-}$ (*Shld3* ^{KO})	Gupta et al.[42]	N/A
Murine: CH12_dRNaseH1-V5	This paper	N/A
Experimental models: Organisms/strains		
Mouse: C57BL6 (WT)	Charles River Laboratories Japan	N/A
Mouse: AID$^{-/-}$	Muramatsu et al.[1]	N/A
Oligonucleotides		
For primers, see Table S4	N/A	N/A
Mouse siHnrnpu	Thermo Fisher Scientific	siRNA ID: MSS225085
Mouse siShld2 5′-CCUGUGUAUGUCUGUGUACCAUGUA	Thermo Fisher Scientific	N/A
Mouse siFen1	Thermo Fisher Scientific	siRNA ID: MSS204267
Recombinant DNA		
Plasmid: HNRNPU-MF (HNRNPU-MF- mKG)	This paper	N/A
Plasmid: HNRNPU (ΔRGG)-MF	This paper	N/A
Plasmid: EGFP-HNRNPU-MF	This paper	N/A
Plasmid: EGFP-ΔRGG-MF	This paper	N/A

(*Continued on next page*)

Continued

REAGENT or RESOURCE	SOURCE	IDENTIFIER
Plasmid: EGFP-NLS-RGG-MF	This paper	N/A
Plasmid: SHLD1-MF	This paper	N/A
Plasmid: dRNase H1-V5	Addgene	cat# 111904
Plasmid: FLAG-tagged KU80	Addgene	cat# 46958
Plasmid: eGFP-tagged 53BP1	Addgene	cat# 60813
Plasmid: FLAG-tagged SFPQ	Addgene	cat# A1360
Plasmid: Halo-tagged FEN1	Promega	cat# FHC03361
pGEM-T Easy vector	Promega	cat# A1360
Software and algorithms		
GraphPad Prism 8	GraphPad	RRID: SCR_002798
BD FACSCalibur Flow Cytometry	BD Biosciences	RRID: SCR_000401
ImageJ	https://imagej.net	RRID: SCR_003070

RESOURCE AVAILABILITY

Lead contact

Further information and requests for resources and reagents should be directed to and will be fulfilled by the lead contact, Tasuku Honjo (honjo@mfour.med.kyoto-u.ac.jp).

Materials availability

All unique reagents generated in this study are available from the lead contact upon a reasonable request without any restriction, or some restrictions (i.e., MTA completion) may apply.

Data and code availability

- Data not included in the main or supplementary figures is available from the lead contact upon request.
- This paper does not report original code.
- Any additional information required to reanalyze the data reported in this paper is available from the lead contact upon request.

EXPERIMENTAL MODEL AND SUBJECT DETAILS

Cell lines

Our study mainly includes mouse B-cell line CH12/CH12F3-2A[39] and its derivative lines such as Bcl2 expressing CH12 line.[102] The *53bp1* ^{KO}, *Shld1* ^{KO} and *Shld3* ^{KO} CH12 lines were previously reported.[42] All cell lines used in this study were included in the Key Resources Table.

The CH12 line expressing catalytically dead RNaseH1 (dRNaseH1) was generated during the course of the present study and described under the Methods. Human embryonic kidney (HEK)-293T cells were obtained from ATCC and used for transient transfection assays.

The CH12 cells were maintained in complete RPMI supplemented with 10% FBS, 5% NCTC, 0.05% 2-mercaptoethanol, and penicillin/streptomycin.[39] HEK293T cells were cultured in complete DMEM supplemented with 10% FBS and penicillin-streptomycin at 37C with 5% CO2.

Mice

Wild type and *Aid*$^{-/-}$ C57BL/6 mice were used under the protocols approved by the Animal Research Committee, Graduate School of Medicine, Kyoto University. Both male and female mice aged 6–8 weeks were used indiscriminately to isolate B cells from splenocytes. Mice were maintained in a specific pathogen-free barrier facility under standardized conditions at the Institute of Laboratory Animals, Graduate School of Medicine, Kyoto University.

Primary B-cells

B lymphocytes were isolated using a mouse B lymphocyte enrichment kit (BD Biosciences) from red blood cell depleted splenocytes prepared from wild type or *Aid*$^{-/-}$ mice. The B cells were cultured in RPMI media supplemented with 10% FBS, 1x MEM non-essential amino acids, 2 mM L-glutamine, 1mM sodium pyruvate, and 0.05% 2-mercaptoethanol at 37C and 5% CO2 levels.

METHOD DETAILS

Gene knockdown transfection

The Bcl2-expressing mouse B-cell lymphoma line CH12F3-2A was cultured as described in the literature.[102] Stealth RNAi siRNA (ThermoFisher) or locked nucleotide acid (LNA) GapmeR ASO (antisense oligonucleotide) (QIAGEN) was used to knockdown specific genes in CH12F3-2A cells. The gene-specific siRNA or ASO was electroporated into the cells (1×10^6) using the SF Cell Line 96-well Nucleofector Kit, according to the manufacturer's guidelines (program CM-150).

In siRNA transfection experiments in primary B cells, isolated B cells were pre-activated with LPS for two days, followed by electroporation with 40 pmol of siRNA (Control or Hnrnpu). Approximately 6-7 $\times 10^5$ cells were used per electroporation with the SF Cell Line 96-well Nucleofector Kit for activated mouse B cells using program # 96-DI- 100.

Transfection in HEK293T cells was performed following the FuGENE 6 transfection reagent (Promega) protocol. Approximately 2.5×10^5 cells were plated in a 6-well plate the day before transfection, and 0.5-1mg of plasmid DNA was used per transfection. The cells were harvested at 48 h post-transfection for the downstream analysis.

Generation and use of stable CH12 lines

To generate stable CH12F3-2A transfectants of catalytically dead RNaseH1 (dRNase H1), the V5-tagged D210N mutant of RNase H1 was transfected into CH12F3-2A cells and subjected to hygromycin B (GIBCO) selection. Hygromycin-resistant clones with good dRNase H1-V5 expression were selected for the downstream experiment.

We used three previously reported gene knockout (KO) CH12F3-2A lines, *53bp1* ^{KO}, *Shld*1 ^{KO}, and *Shld3* ^{KO}.[42] The CRISPR/CRISPR-associated protein 9 (Cas9)-mediated disruption of the target locus was confirmed by sequencing a single cell clone from each KO line (Figures S2A–S2C). We also confirmed that no WT transcript could be detected in the *Shld1* ^{KO} and *Shld3* ^{KO} lines (Figure S2D). Similarly, no expression of 53BP1 was observed in the *53bp1* ^{KO} line (Figure S1H).

Constructs and mutagenesis

The *HNRNPU* coding DNA sequence (NM_016805.3) was PCR amplified from an Addgene plasmid (#38068) and cloned into the *Mlu* I/*Asi*S I sites of the pCMV6-Entry mammalian expression vector (OriGene) to generate an MYC-FLAG-tag (MF) fusion at the C-terminus of HNRNPU. The monomeric Kusabira-GFP gene fragment (mKG_C) was added in frame with MF by cloning into the *Kpn* I/*Eco*R I sites of the phmKGC-MN mammalian expression vector (AM-1100; MBL). The final construct was designated HNRNPU-MF and was used as a template to generate the *HNRNPU* mutant ΔRGG-MF.

For construction of MYC-FLAG epitope-tagged and EGFP fused HNRNPU, the MYC-FLAG epitopes DNA sequence of HNRNPU was cloned into the SalI/HindIII sites of the pEGFP-C1 vector (Clontech). The Q5 Site-Directed Mutagenesis Kit was used to delete the RNA-binding RGG domain. To construct C-terminally epitope-tagged SHLD1, the coding DNA sequence (NM_001358260.2) of the *Shld1* gene was obtained by RT-PCR of the total RNA extracted from CH12F3-2A cells. The PCR product was cloned into the *Mlu* I/*Asi*S I sites of the pCMV6-Entry vector (OriGene) in frame with MYC-FLAG. All constructs were verified by Sanger sequencing.

CSR assay in CH12 and primary B cells

To induce IgM to IgA antibody class switching, CH12F3-2A cells were treated with CD40 L, IL4, and TGFβ (CIT)[39] for 24 h or 48 h. The CIT-stimulated cells were surface stained with FITC-conjugated anti-mouse IgM (Invitrogen) and PE-conjugated anti-mouse IgA (Southern Biotech) antibodies. Cells were also stained with propidium iodide to exclude dead cells. Flow cytometry data acquisition was performed on a BD FACS Calibur, and post analysis was performed using either BD FlowJo or BD CellQuest software.

Following siRNA electroporation, primary B cell cells were cultured in the presence of LPS and IL4 for three days[1] and then surface stained with an anti-IgG1 biotinylated antibody in combination with allophycocyanin-labeled streptavidin.[103,104] Dead cells were excluded from analysis by gaiting propidium iodide-positive cells.

Immunoprecipitation and immunoblotting

For immunoprecipitation (IP) of endogenous HNRNPU, nuclear extracts were prepared from CH12F3-2A cells stimulated for 24 h with CIT following the manufacturer's instructions for NE-PER Nuclear and Cytoplasmic Extraction Reagents. Nuclear extracts were divided and incubated with Protein G Dynabeads precoated with an anti-HNRNPU antibody or negative control IgG antibody overnight at 4°C. For the SHLD1 immunoprecipitation, CH12F3-2A cells were transiently transfected with SHLD1-MF and stimulated 24 h later with CIT and incubated for another 24 h. Nuclear extracts were prepared as described, and anti-FLAG IP was performed using Protein G Dynabeads precoated with the anti-FLAG M2 antibody. For IP using 293T cells, anti-FLAG IP was performed using nuclear extract from cells transfected with the indicated FLAG-tagged construct. All immunoprecipitated samples were washed three times with modified RIPA buffer (30 mM Tris·HCl; pH 7.4; 150 mM NaCl; 10% glycerol; 0.05% sodium deoxycholate; 5 mM EDTA and 1% Triton X-100) supplemented with EDTA-free protease inhibitors. Immunoprecipitated samples were untreated or treated with RNase A for 30 min at 37°C. The immunoprecipitants (bead-bound) were heated at 85°C for 10 min in the presence of 1X SDS sample buffer.

For whole-cell protein extraction, cells were washed and lysed on ice with modified RIPA buffer supplemented with EDTA-free protease inhibitors. The extract was centrifuged at 15,000 rpm for 10 min at 4°C. The final samples were prepared with 1X SDS sample buffer and heated at 85°C for 10 min.

For immunoblotting, heated samples suspended in 1x SDS buffer were size separated on a 4–20% Mini Protein TGX Precast Gel (BioRad #4561096) and transferred to a PVDF membrane (Amersham #10600003). The membranes were blocked with 5% nonfat milk and immunoblotted using the primary and secondary antibodies (HRP-conjugated) as needed. The signal was developed using chemiluminescence reagents, and protein bands were visualized using an LAS 4000 imaging system.

Isolation of HNRNPU- or SHLD1-bound RNA and RT–qPCR

For extraction of RNA from the immunoprecipitated complex, nuclear extract was prepared using NE-PER Kit from CH12F3-2A cells stimulated for 24 h with CIT (Figure S9) or from 293T cells transfected with either HNRNPU-MF or SHLD1-MF construct (Figure 6C). This extract was subjected to HNRNPU-IP or FLAG-IP in CH12F3-2A and 293T cells, respectively, using precoated Protein G Dynabeads with HNRNPU, FLAG or IgG antibody. The beads were washed with ice-cold Magna Immunoprecipitation (RIP) buffer (Merck Millipore #17–700) supplemented with EDTA free protease inhibitors and RNase Inhibitor. The RNA–protein complex-bound beads were subjected to protein and RNA extraction in duplicate. For immunoblotting, HNRNPU/SHLD1-IP beads were heated with 1X-SDS sample buffer for Western blotting. For total RNA extraction, beads were suspended in TRIzol reagent, and subsequently, RT–qPCR was performed using the primer set listed in Table S4.

Class-switch recombination junction analysis

For Sμ-Sα recombination junction analysis, CH12F3-2A cells were stimulated with CIT for 48 h, and IgA (+) cells were isolated using anti-PE Magnetic Particle-DM, followed by genomic DNA extraction. The junctions from switched cells were amplified by nested PCR with the Sμ- and Sα-specific primers listed in Table S4. PCRs were performed using PrimeSTAR HS DNA Polymerase. The PCR conditions for the first PCR were 95°C for 2 min, 98°C for 10 s, and 68°C for 7 min for a total of 22 cycles with the first-round primers. After purifying the PCR products, the resulting DNA was subjected to 23 cycles of a second PCR (95°C for 2 min, 98°C for 10 s, and 68°C for 1 min and 20 s) using the second-round primers. PCR products between 0.3 and 1.5 kilobases were gel-extracted, A-tailed by Taq DNA Polymerase, and TA-cloned into the pGEM-T Easy vector. The plasmids obtained from individual colonies were sequenced using T7 forward and Sp6 reverse universal primers with an ABI PRISM 3130xl Genetic Analyzer (Applied Biosystems). To identify junctions, the sequence was aligned against mouse μ (AH005309.2) and α (D11468.1) switch region sequences of immunoglobulin genes using pairwise nBLAST in the NCBI database. The detailed number and sequences of the analyzed CSR junctions per genotype are shown in Tables S1 and S2.

Analysis of S-region SHM

For S-SHM analysis, genomic DNA was isolated from CH12F3-2A cells after 48 h of CIT stimulation followed by PCR amplification using PrimeSTAR DNA polymerase with the following amplification conditions: 95°C for 5 min, 30 cycles at 98°C for 10 s, 55°C for 5 s, and 72°C for 1 min. Purified PCR fragments were A-tailed by Taq DNA Polymerase, cloned into pGEM-T Easy vector, and sequenced using T7 forward and Sp6 reverse universal primers, as described above. Mutations were analyzed over 565 bp from the Sμ region using the Sequencher DNA software (Gene Codes). The mutation frequency was calculated from the number of mutations per total bases analyzed. The primers used for SHM analysis are listed in Table S4.

IgH/c-Myc chromosomal translocation analysis

CH12F3-2A cells were stimulated with CIT for 48 h, and genomic DNA was purified by phenol:chloroform extraction. *IgH/c-Myc* translocation junctions (der15) were PCR-amplified using nested PCR, as described.[105,106] Several aliquots of DNA (750 ng/reaction) were analyzed (24 reactions/sample) using the Expand Long Template PCR System. The first PCR conditions were 94°C for 3 min, 94°C for 15 s, 62°C for 15 s, 68°C for 7 min and 20 s per cycle for 25 cycles, and 5 min at 68°C for a final extension. The second round of PCR was similar to the first round, except the extension was only 7 min. After the PCR products were electrophoresed on EtBr-treated gels, southern blotting was performed using *c-Myc* locus-specific probes. The sequences of the primers and *c-Myc* probe are shown in Table S4.

RNA extraction, cDNA synthesis, and quantitative RT–PCR

Total RNA was isolated from CH12F3-2A cells using TRIzol (Gibco BRL), and cDNA was synthesized from 1 μg of total RNA using SuperScript IV reverse transcriptase. PowerUp SYBR Green Master Mix was used for the quantitative real-time PCR (RT-PCR) with an RT-PCR system (Applied Biosystems). Gene expression was normalized to *Gapdh* and calculated using the $2^{-\Delta\Delta CT}$ method. The primers used for qPCR are listed in Table S4.

Double-strand DNA break detection by LM-PCR

Gene knockout or knockdown CH12F3-2A cells were stimulated for CSR, and Sμ DNA breaks were analyzed using established methods.[107–109] Briefly, the ligation of the dsDNA oligo-linker into the genomic DNA was performed in the processed cells embedded in the low-melting temperature agarose plugs. The ligation reaction proceeded overnight at 16°C, followed by inactivating of the T4

DNA ligase by heating the samples at 70°C to the linker-ligated DNA was subjected to PCR using KOD FX *Neo* DNA polymerase and an Sμ-specific and linker-specific nested primer set. Nonisotopic Southern blotting of the PCR products was performed using a DIG-labeled Sμ probe and following the standard protocol. The amount of genomic DNA input was monitored by *Gapdh* gene locus-specific PCR. The sequences of the primers and probes are described.

Chromatin immunoprecipitation (ChIP) assay

We used the ChIP-IT Express Kit with minor modifications. Briefly, 5×10^6 CH12F3-2A cells were fixed with 1% formaldehyde for 8 min at room temperature. The reaction was quenched by adding 0.125 M glycine, and the crosslinked cells were lysed for 10 min at 4°C with rotation. The nuclei were resuspended in shearing buffer and sonicated on a Bioruptor (Diagenode) to generate fragments ranging in size from 200 to 1000 bp. The soluble crosslinked chromatin fraction was immunoprecipitated overnight with 3–5 μgof antibodies and Protein A/G magnetic beads at 4°C with rotation. The bead-bound chromatin was extensively washed, and the bound chromatin was eluted according to the manufacturer's instructions. Immunoprecipitated DNA was analyzed by quantitative RT-PCR using the Power SYBR Green Master Mix and normalized to the amount of input DNA.[102] The primers used for ChIP analysis in primary B cells was described.[110]

DNA–RNA immunoprecipitation (DRIP)

The DRIP assay for the IgH locus was adopted from previously developed methods.[111,112] Briefly, genomic DNA was extracted from activated CH12F3-2A cells transfected with nonspecific control or gene-specific siRNA. Genomic DNA (50 μg) was digested with a restriction enzyme cocktail (*Hin*d III, *Eco*R I, *Xba* I, *Ssp* I, *Bsr*G I) in digestion buffer (10 mM Tris-HCl pH 8; 10 mM MgCl2; 50 mM NaCl; 1 mM dithiothreitol (DTT) overnight at 37°C followed by RNase A treatment and the purification of the genomic DNA by phenol–chloroform. Digested DNA (6 μg) was either untreated or treated with RNase H overnight at 37°C. The RNase H-treated and untreated genomic DNA samples were incubated overnight with the S9.6 antibody (1 μg/μL) in DRIP buffer (10 mM NaPO4 pH 7.0; 140 mM NaCl; 0.1% Triton X-100) at 4°C, followed by further incubation for 3 h with 30 μL of Protein G Dynabeads at 4°C. The antibody DNA complexes bound to Protein G Beads were washed three times with DRIP buffer and once with TE buffer (20 mM Tris-HCl pH 8; 1 mM EDTA) and eluted twice with 60 μL of elution buffer (100 mM NaHCO3; 1% SDS). Proteinase K was added to eluted DNA, and finally, the DNA–RNA hybrids were purified using a DNA purification kit. Quantitative RT-PCR was performed using the primers listed in Table S4, and the DRIP-qPCR/input ratio was used to calculate the enrichment.

Immunofluorescence (IF) staining

For the IF experiment, 293T cells were seeded in 8-well chamber slides (ThermoFisher, #155411) for 24 h prior to EGFP-fused HNRNPU transfection. Transfected cells were treated with 100 μM etoposide for 30 min to induce DNA damage. Immunofluorescence staining was conducted as previously described.[113] Briefly, after etoposide treatment, the cells were washed with PBS and pre-extracted for 4 min with CSK extraction buffer (10 mM Pipes, pH 7.0, 100 mM NaCl, 300 mM sucrose, 3 mM MgCl2, and 0.7% Triton X-100) at room temperature, followed by fixation with 4% paraformaldehyde (PFA) for 10 min and permeabilization with 0.5% Triton X-100 in PBS for 10 min at room temperature. Cells were washed with PBS, blocked with 1% BSA-PBS for 30 min, and incubated at room temperature for 2 h with primary antibodies diluted in blocking solution: anti-γ-H2AX, anti-KU80, and anti-53BP1. After washing, secondary antibodies (Alexa Fluor 674) were added and incubated at room temperature for 1 h. After washing three times with PBS, the slides were mounted in media containing DAPI. Cells were visualized using a Nikon ECLIPSE Ti2 microscope, followed by a co-localization study performed by Nikon's NIS-Elements software, as described.[114]

Biotinylated SμG4 RNA/DNA oligonucleotide pull-down assay

The stepwise workflow of the assay is depicted in detail in Figures S6D and S6F. Synthetic 5′-biotinylated RNA oligonucleotides (Sμ4G-RNA and $S\mu4G^{mut}$-RNA) and DNA oligonucleotide (Sμ4G-ssDNA) shown in Figure S6E were purchased from Integrated DNA Technologies (IDT). The pull-down assay was performed as described before.[60] Briefly, the b-oligonucleotides were diluted to the final concentration of 5 μM in a buffer containing 100 mM KCl or LiCl buffer and heated at 95°C for 5 min, followed by slow cooling to room temperature at a rate of 0.5 °C/s in a thermal cycler. The folding of the b-oligonucleotides was confirmed by running the samples on 10% native polyacrylamide gels and stained with SYBR Gold (Thermo Fisher). To prepare the cell extract, CH12F3-2A cells stimulated with CIT for 24 h were lysed in RIPA buffer supplemented with protease inhibitor (Roche). The b-oligonucleotide pull-down assay, using the clarified cell extract, was carried out by Dynabeads M-280 streptavidin beads (25 μL/assay). The beads were washed four times with RIPA buffer and once with PBS and divided into two equal fractions for examining the bound b-oligonucleotides and proteins by slot blot and immunoblot analysis, respectively. We noticed that HNRNPU was readily detected in our b-oligonucleotide pull-down assay at various concentrations of the cell extract ranging from $0.5\text{-}1\times10^7$ cells/mL. However, AID detection strictly requires a higher concentration of CIT-stimulated CH12F3-2A cell extract (5×10^7 cells/mL), possibly due to its relatively low abundance.

293T cells expressing EGFP fused and Myc-FLAG epitope-tagged HNRNPU (WT or mutant) were lysed in the same lysis buffer as for CH12F3-2A cell lysis. Anti-FLAG-IP was performed using FLAG-agarose beads (20 μL/assay) to immunoprecipitate EGFP-HNRNPU-MF proteins or the EGFP-HF protein as a negative control. After five successive washes, the immunoprecipitated beads

were suspended in the oligonucleotide pull-down assay buffer and incubated with pre-folded oligos. All downstream steps, including the extraction and detection of bound protein and RNA/DNA oligonucleotides, were performed as described.[60]

Biotinylated isoxazole-mediated HNRNPU precipitation assay

The b-isox precipitation assay was conducted according to previously described protocols.[70,115] Whole-cell extracts were prepared from unstimulated and CIT-stimulated CH12F3-2A cells. Approximately 1-1.5 × 10^7 cells were suspended in 1 mL of lysis buffer (20 mM Tris-HCl pH 7.4, 300 mM NaCl, 5 mM MgCl2, 1% NP40, 10% glycerol, 20 mM β-mercaptoethanol) supplemented with protease inhibitor (EDTA free) and a protein phosphatase inhibitor mix containing vanadate and NaF. Cells were first kept on ice for 30 min, followed by a brief sonication (Bioruptor) centrifugation at 4°C, 15,000 x g for 20 min. The clear supernatant was aliquoted equally into a low protein binding Eppendorf tube. The aliquots were mixed with b-sox and rotated at 4°C for 30–60 min. Various concentrations of b-isox were tested, ranging from 10 μM to 200 μM. B-isox precipitates were collected by centrifugation for 15 min at 4°C. Pellets were washed (4x) with the lysis buffer supplemented with EDTA-free protease inhibitor and RNaseOUT. The final pellet, suspended in 1x SDS sample buffer containing β-mercaptoethanol, was heated at 95°C for 8 min and subjected to Western blot analysis. All fractions, including input, pellet, and post-pellet supernatant, were monitored during the initial optimization. Since b-isox was dissolved in DMSO, we also treated the cell extract with an identical concentration of DMSO as a control, which did not precipitate HNRNPU. The same protocol was adapted for 293T cells transfected with various HNRNPU constructs, as illustrated in Figures S8A and S8B.

QUANTIFICATION AND STATISTICAL ANALYSIS

Statistical significance was determined using an unpaired Student's t-test using Prism 8 (GraphPad Software). In all cases, ns: not significant ($p > 0.05$),*: $p < 0.05$, **: $p < 0.01$, ***: $p < 0.001$, and ****: $p < 0.0001$. Figure legends indicate the number of replicates for each experiment and if data are represented as means or medians ±SD.